

Cytosolic FKBPL and ER-resident CKAP4 co-regulates ER-phagy and protein secretion

Received: 26 May 2022

Accepted: 27 August 2024

Published online: 09 September 2024

Cathena Meiling Li¹, Jaemin Kang¹, Jongyeon Baek¹, Youbin Kim²,
Heemin Park¹ & Yong-Keun Jung^{1,2}✉

Endoplasmic reticulum quality control is crucial for maintaining cellular homeostasis and adapting to stress conditions. Although several ER-phagy receptors have been identified, the collaboration between cytosolic and ER-resident factors in ER fragmentation and ER-phagy regulation remains unclear. Here, we perform a phenotype-based gain-of-function screen and identify a cytosolic protein, FKBPL, functioning as an ER-phagy regulator. Over-expression of FKBPL triggers ER fragmentation and ER-phagy. FKBPL has multiple protein binding domains, can self-associate and might act as a scaffold connecting CKAP4 and LC3/GABARAPs. CKAP4 serves as a bridge between FKBPL and ER-phagy cargo. ER-phagy-inducing conditions increase FKBPL-CKAP4 interaction followed by FKBPL oligomerization at the ER, leading to ER-phagy. In addition, FKBPL-CKAP4 deficiency leads to Golgi disassembly and lysosome impairment, and an increase in ER-derived secretory vesicles and enhances cytosolic protein secretion via microvesicle shedding. Taken together, FKBPL with the aid of CKAP4 induces ER fragmentation and ER-phagy, and FKBPL-CKAP4 deficiency facilitates protein secretion.

The endoplasmic reticulum (ER) is the largest membranous subcellular organelle, playing crucial roles in protein and lipid synthesis, detoxification, calcium storage, and protein sorting for secretion, etc.^{1–5}. Moreover, cellular homeostasis is partly maintained through tightly regulated ER quality control. When unfolded or misfolded proteins accumulate in the ER, it increases ER stress and activates the unfolded protein response (UPR)⁶. To alleviate this burden, misfolded proteins are eliminated through ER-associated degradation (ERAD), ER-phagy, and protein secretion^{7–11}. ERAD involves translocating misfolded proteins into the cytosol via an ER membrane complex for degradation by the ubiquitin-proteasome system⁸. However, ERAD handles only a small fraction of the misfolded proteins; the majority are managed through ER-phagy and protein secretion.

ER-phagy is a form of selective autophagy where malfunctioning portions of the ER are sequestered into the autophagosomes for lysosomal degradation¹². Autophagy receptors interact with autophagosome-conjugated Atg8/LC3/GABARAP via Atg8-interacting motif (AIM) in yeast or LC3-interacting region (LIR) motif or GABARAP-

interacting motif (GIM) in mammals, selectively degrading cargoes^{12,13}. These receptors can serve as cargo themselves or as mediators delivering cargo into autophagosomes. Several ER-phagy receptors have been identified in mammals, including ER-resident membrane proteins and soluble proteins in the cytosol^{14–22}. They regulate ER-phagy in a spatiotemporal and tissue-specific manner. In some cases, combinations of cytosolic and ER-resident factors, such as p62-TRIM13 and CALCOCO1-VAPs in mammals and Erp1-VAPs in fission yeast, work together to mediate ER-phagy^{21–23}. However, how cytosolic ER-phagy receptor facilitates ER fragmentation and ER-phagy remains unknown.

Some ER stress inducers, like Ca²⁺ ionophore A23187, dithiothreitol (DTT), and tunicamycin (TM), lead to the accumulation of misfolded and unfolded proteins, subsequently inducing ER-phagy^{15,17}. Besides the accumulation of misfolded and unfolded proteins, autophagy induction by mTOR inhibitor and nutrient starvation also trigger receptor-mediated ER-phagy^{14,16,18–20}. ER membrane curvature formation and ER fragmentation are prior to ER-phagy. Reticulon domain retained in ER-phagy receptors, the accumulation of misfolded

¹School of Biological Sciences, Seoul National University, Gwanak-gu, Seoul, Korea. ²Interdisciplinary Program in Neuroscience, Seoul National University, Gwanak-gu, Seoul, Korea. ✉e-mail: ykjung@snu.ac.kr

proteins and scaffolding proteins facilitate ER fragmentation. However, the collaboration between cytosolic and ER-resident proteins under ER stress and fragmentation, as well as their roles in cargo recognition, remains to be elucidated.

Secretory proteins are transported to the extracellular space via the ER-to-Golgi trafficking pathway. Cells can also generate various types of secretory vesicles, including exosomes and microvesicles, which differ in biogenesis, components, and size²⁴. Exosomes are generated by the invagination of endolysosomal vesicles, called the multivesicular body (MVB)²⁵. Microvesicles are shed from the outward budding of the plasma membrane, and the activation of the small GTPase ADP ribosylation factor 6 (ARF6) leads to the budding and pinching off of the plasma membrane²⁶. In addition, the inhibition of lysosome activity facilitates protein secretion via autophagosomes²⁷.

In this study, we designed and performed a phenotype-based gain-of-function screen. We then focused on a cytosolic protein FKBPL carrying multiple protein-binding domains. Through association with CKAP4, an ER-resident transmembrane protein, FKBPL contributes to ER fragmentation, ER-phagy, and even protein secretion. These results highlight the collaboration between cytosolic and ER-resident factors in regulating ER-phagy and protein secretion, and in modulating ER stress and cytosolic cues.

Results

A gain-of-function screen identifies FKBPL as a novel ER fragmentation regulator

To identify a novel ER-phagy receptor, we searched ~2000 ER-resident proteins in the NCBI database and checked for the presence of potential LIR motifs using the prediction program iLIR and hFAIM^{28,29}. We found 442 potential LIR-containing ER proteins and collected 135 cDNAs encoding potential ER-phagy receptor candidates (Supplementary Fig. S1a and Supplementary Table 1). We then examined the phenotype of ER-phagy by co-transfecting the ER marker RFP-KDEL and FAM134B, a known ER-phagy receptor¹⁴, and observed increased ER fragmentation in Hep3B cells (Fig. 1a and Supplementary Fig. S1b, c). Based on this phenotype, we screened the 135 candidates and found that overexpression of FK506-binding protein (FKBP) prolyl isomerase-like (FKBPL) increased ER fragmentation (Fig. 1a and Supplementary Fig. S1b, c). In vertebrates, FKBPL is a member of the FKBP protein family, which shows sequence similarity to the immunophilin protein family^{30,31}. Among the members of the FKBP protein family, only FKBPL induced a significant increase in ER fragmentation in the transfected Hep3B cells (Supplementary Fig. S1d).

FKBPL mediates ER turnover via selective autophagy

To elucidate the role of FKBPL in ER-phagy, we examined the endogenous level of FKBPL in several cell lines and found that Hep3B cells expressed little FKBPL compared to HEK293T and HeLa cells (Supplementary Fig. S2). Therefore, we conducted overexpression experiments mainly in Hep3B cells. We discovered that the ER fragments generated by FKBPL overexpression co-localized with LAMP1-GFP, a lysosome marker (Fig. 1b and Supplementary Fig. S3a, c), and GFP-LC3B, an autophagosome marker (Fig. 1c and Supplementary Fig. S3b, c). In addition, we observed abnormally fragmented ER engulfed in double-membrane autophagosomes/autolysosomes under an electron microscope in FKBPL-overexpressing cells (Supplementary Fig. S3d). We also developed a pH-dependent ER-phagy reporter, mKeima-SEC61B, in which the monomeric pH-sensitive protein Keima (mKeima) is conjugated to the translocon component SEC61B. The mKeima is a dual-excitation ratiometric protein (550/438 nm)³². Puncta excited at 440 nm represents pH > 7.0, while excitation at 550 nm indicates pH < 5.5 (Fig. 1d)³³. Overexpression of FKBPL increased the numbers of acidic mKeima-SEC61B puncta (Fig. 1e, f). We also measured ER-phagic flux using a doxycycline-inducible reporter protein ssRFP-EGFP-KDEL, which is cleaved by lysosomal hydrolases²⁰.

Overexpression of FKBPL increased the levels of the cleaved relative to the full-length ssRFP-EGFP-KDEL, and this was inhibited by the V-ATPase inhibitor bafilomycin A1 (Baf. A1) (Fig. 1g–i). Thus, excessive expression of FKBPL induces both ER fragmentation and ER-phagy.

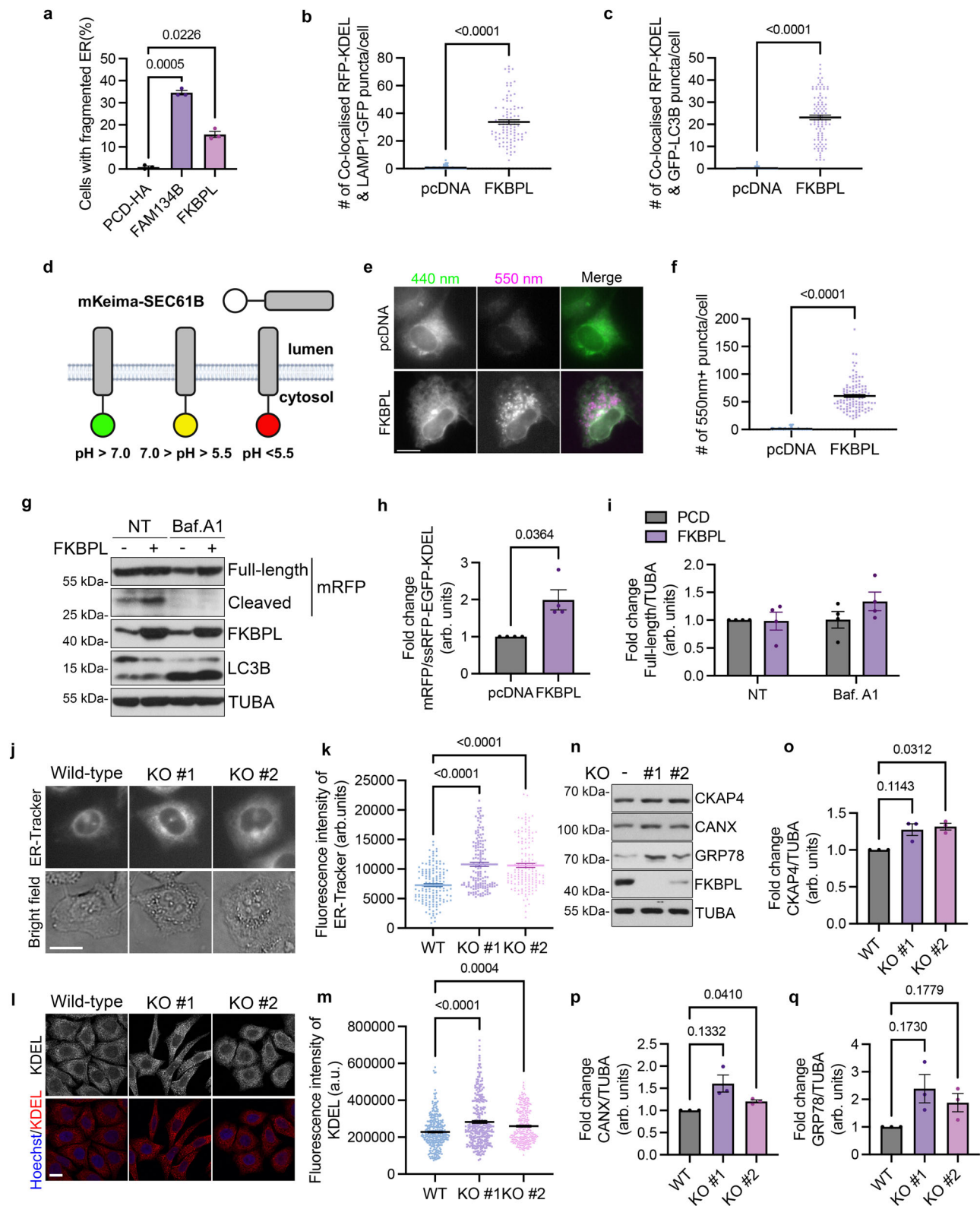
To better understand the role of FKBPL in ER-phagy regulation, we generated FKBPL knockout (KO) cell lines using a CRISPR-Cas9 system³⁴. HeLa/FKBPL KO cells showed enhanced fluorescence intensities of ER-Tracker and the ER marker KDEL (Fig. 1j–m), as well as intriguing vacuolized membrane phenotypes (Fig. 1j). Loss of FKBPL also led to the accumulation of the ER-resident membrane protein CKAP4 and ER-resident chaperones CANX and GRP78 (Fig. 1n–q). Taken together, these findings suggest that FKBPL plays a crucial role in ER-phagy regulation.

FKBPL interacts with the members of LC3/GABARAP via two LIR motifs

According to the LIR motif prediction program^{28,29}, FKBPL contains two potential LIR motifs, ₁₄₁WTEL₁₄₄ and ₁₅₆WGEL₁₅₉, referred to as LIR1 (amino acids 141–144) and LIR2 (amino acids 156–159), respectively (Fig. 2a). Using an overexpression immunoprecipitation (IP) assay, we found that FKBPL exhibited binding affinities for LC3A, LC3B, and LC3C, and GABARAP1 among the six members of LC3/GABARAP family (Fig. 2b). We then generated three LIR mutants, FKBPL mutLIR1 (ATEA), FKBPL mutLIR2 (AGEA), and FKBPL mutLIR1/2 (ATEA AGEA) (Fig. 2a). The first and fourth amino acids of the putative LIR motifs, which are essential for LC3/GABARAP interaction³⁵, were replaced with alanine. Subsequent cellular-binding assays revealed that only FKBPL mutLIR1/2, harboring mutations in both LIR motifs, failed to bind to LC3B (Fig. 2c), indicating that both LIR motifs are crucial for LC3/GABARAP interaction. In addition, FKBPL mutLIR1/2 was less able to increase the number of acidic mKeima-SEC61B puncta compared to FKBPL WT (Fig. 2d, e). Since cell fixation leads to a loss of fluorescence signal of mKeima, we measured ER-phagy induction using doxycycline-inducible HeLa/ssRFP-EGFP-KDEL²⁰. Because GFP fluorescent signal is quenched in acidic conditions, RFP-only puncta represent degrading ones, while GFP⁺RFP⁺ puncta indicate ER fragments before degradation²⁰. Although both FKBPL WT and mutLIR1/2 induced ER fragmentation, only FKBPL WT, and not FKBPL mutLIR1/2, showed degrading RFP-only puncta (Fig. 2f). Thus, the two LIR motifs in FKBPL are functional for both the interaction with LC3/GABARAP and the induction of ER-phagy.

CKAP4 is an ER-resident receptor for FKBPL

Topological analysis revealed that GFP-FKBPL rapidly lost fluorescence signals, while the ER marker RFP-KDEL was resistant to degradation (Supplementary Fig. S4a), suggesting that FKBPL is localized in the cytosol. Despite lacking a signal peptide sequence and transmembrane domain, FKBPL was also detected in the ER fractionation (Supplementary Fig. S4b). This led us to hypothesize that FKBPL requires an ER membrane protein for docking at the ER. To identify a potential ER-resident interacting partner, we performed affinity purification coupled with mass spectrometry (AP-MS) using FKBPL as bait (Supplementary Fig. S5a). Among the identified peptides, we focused on three top-rated ER membrane proteins, dolichyl-diphosphooligosaccharide-protein glycosyltransferase (RPN1), calnexin (CANX), and cytoskeleton associated protein 4 (CKAP4), for further characterization (Supplementary Fig. S5b). To assess the binding affinity between FKBPL and these candidates, we generated a biotin ligase-conjugated construct, V5-APEX-FKBPL. This construct allows biotinylation of proteins within a 20 nm proximity (Fig. 3a)³⁶. Among the candidates, only CKAP4 was biotinylated by V5-APEX-FKBPL, whereas RPN1 or CANX were not (Fig. 3b). This interaction was further confirmed through IP analysis, which demonstrated that CKAP4 specifically interacts with FKBPL (Fig. 3c, d). CKAP4, a multimeric type II transmembrane protein with luminal coiled-coil domains, plays multiple roles, including organizing ER membrane structure and anchoring the ER to microtubules^{37–39}.



To identify the specific regions involved in the FKBPL-CKAP4 interaction, we generated a series of FKBPL and CKAP4 deletion (Δ) mutants (Fig. 3e, g)⁴⁰. IP analysis revealed that deletion of both the middle portion of FKBPL (Δ 86–209) and the tetratricopeptide (TRP) domain (Δ 210–319) abolished its interaction with CKAP4 (Fig. 3f). Similarly, deletion of residues spanning 60–105 (Δ 60–105) in CKAP4, which is exposed to the cytosolic side, disrupted the FKBPL-CKAP4 interaction (Fig. 3h). Interestingly, FKBPL itself was also biotinylated,

indicating that it might self-associate (Fig. 3b). This self-association was confirmed by overexpression IP assay (Supplementary Fig. S6a). Domain mapping revealed that the TPR domain is essential for self-interaction, while the 86–209 domain partially interferes with this interaction (Supplementary Fig. S6b, c). Despite the requirement of lysine 287 and arginine 291 in the TPR domain for HSP90 α interaction³¹, the FKBPL mutTPR (K287A R291A) mutant still self-associated and interacted with CKAP4 and LC3B (Supplementary Fig. S7). Comparing

Fig. 1 | FKBPL mediates ER turnover through autophagy. **a** Ratio in cells with fragmented ER were quantified. **b, c** Numbers of co-localized RFP-KDEL and LAMP1-GFP (**b**) puncta or GFP-LC3B (**c**) puncta were quantified. **d** Schematic representation of mKeima-SEC61B assessing ER-phagic flux. When $\text{pH} > 7.0$, mKeima-SEC61B excites only at 440 nm, representing green; when $7.0 > \text{pH} > 5.5$, it excites both at 440 nm and 550 nm, representing orange; when $\text{pH} < 5.5$, excites only at 550 nm, representing as red. The illustration created with BioRender.com is released under a Creative Commons Attribution-NonCommercial-NoDerivs 4.0 International license <https://creativecommons.org/licenses/by-nc-nd/4.0/deed.en>. **e, f** Hep3B cells were co-transfected with mKeima-SEC61B and pcDNA3 or FKBPL and observed by fluorescence microscope (**e**). Numbers of 440 nm/550 nm⁺ puncta were quantified. **g–i** HEK293T cells were co-transfected with doxycycline-inducible ssRFP-EGFP-KDEL and pcDNA3.0 or FKBPL for 14 h and cells were maintained in full media containing 10 $\mu\text{g}/\text{ml}$ doxycycline for another 8 h. Cell extracts were analyzed by

immunoblotting (**g**). Signal intensities of cleaved relative to full-length ssRFP-EGFP-KDEL were quantified (**h**). Signal intensities of full-length ssRFP-EGFP-KDEL relative to TUBA were quantified (**i**). **j, k** HeLa/WT or FKBPL KO cells were stained with 1 μM ER-tracker for 30 min and observed by fluorescence microscope (**j**). Fluorescence intensities were measured by ImageJ (**k**). **l, m** HeLa/WT or FKBPL KO cells were fixed, immunostained with anti-KDEL antibody, and observed by confocal microscope (**l**). The fluorescence intensities were measured by ImageJ (**m**). **n–q** Extracts of HeLa/WT or FKBPL KO cells were analyzed by immunoblotting (**n**). Signal intensities of CKAP4 (**o**), CANX (**p**), and GRP78 (**q**) relative to TUBA were quantified. Scale bars in (**e, j, l**) are 10 μm . Data represent the mean \pm SEM of three independent experiments in (**a–c, f, k, m, o, p, q**) and four independent experiments in (**h** and **i**). Differences were statistically analyzed by two-tailed *t* test in (**b, c, f**, and **h**) and by one-way ANOVA followed by Dunnett's multiple comparisons test in (**a, i, k, m, o, p**, and **q**). Arbitrary units, arb. units.

the predicted protein structures of FKBPL using AlphaFold^{41,42}, we observed that it maintains a curved structure in the middle region across different species (Fig. 3i). Notably, deletion of the unstructured region ($\Delta 2\text{--}85$) in FKBPL enhanced its interaction with CKAP4, though it did not affect self-interaction (Fig. 3f and Supplementary Fig. S6c). These findings suggest that the concave of the curve structure provides a binding pocket for CKAP4, which is gated by the N-terminal unstructured region, while FKBPL self-associates via the TPR domain at the bulge of the curve structure (Fig. 3i).

To determine if CKAP4 is essential for the ER localization of FKBPL, we created CKAP4 KO cell lines (Supplementary Fig. S8). In CKAP4 KO cells, FKBPL exhibited reduced localization at the ER (KDEL) compared to WT cells (Supplementary Fig. 9a, b). Furthermore, membrane fractionation using a continuous iodixanol gradient revealed that CKAP4 loss disrupted membrane attachment of FKBPL and shifted its distribution from heavier to lighter fractions (Fig. 3j). However, the ER residency of CKAP4 itself was not affected by FKBPL (Supplementary Fig. S9c). These findings suggest that CKAP4 functions as an ER-resident receptor for FKBPL.

CKAP4 is required for ER-resident cargo recognition

In comparison to WT cells, both ER fragmentation and ER-phagic flux induced by FKBPL overexpression were reduced in Hep3B/CKAP4 KO cells (Fig. 4a–d). This suggests that CKAP4 is also necessary for the induction of ER-phagy. CKAP4 has a relatively large luminal region, which may function as a cargo recognition domain. To explore the role of CKAP4 in cargo recognition, we examined its binding to 10 secretory proteins based on data from the BioGRID interaction repository. We found that CKAP4 binds to all of these proteins (Supplementary Fig. S10a). Domain mapping analysis confirmed that the luminal domain of CKAP4 is essential for interactions with CKAP4-binding partners, such as dickkopf-1 (DKK1) and family with sequence similarity 20, member C (FAM20C) (Supplementary Fig. S10d, e)^{43,44}. In addition, we observed a similar binding pattern of CKAP4 with brain-derived neurotrophic factor (BDNF) and collagen type II alpha 1 chain (COL2A1) (Supplementary Fig. S10b, c).

To further investigate CKAP4-dependent cargo recognition, we examined the role of ER chaperone glucose-regulated protein 78 (GRP78) and collagen type I alpha 2 chain (COL1A2). GRP78 assists in preventing the aggregation of nascent polypeptides and facilitates their proper folding⁴⁵. Treatment with tunicamycin (TM), which disrupts protein glycosylation in the ER lumen⁴⁶, leads to an increase in misfolded proteins and clustering of GRP78, indicating the presence of misfolded proteins. As anticipated, TM treatment in the presence of Baf. A1 increased the numbers of GRP78-positive puncta, some of which co-localized with FKBPL in WT cells (Fig. 4e, f). In contrast, CKAP4 KO cells showed a reduction in both the numbers of GRP78-positive puncta and their co-localization with FKBPL (Fig. 4e–g). Similarly, COL1A2-positive puncta and their co-localization with FKBPL were observed but were also reduced in CKAP4 KO cells (Fig. 4h–j).

These findings suggest that CKAP4 is crucial for linking FKBPL with cargoes in the ER lumen.

FKBPL-CKAP4 interaction and FKBPL oligomerization are essential for stress-induced ER-phagy

In HeLa/ssRFP-EGFP-KDEL cells, the loss of FKBPL and/or CKAP4 led to a reduction in ER-phagic flux (Fig. 5a–f). To investigate the collaborative roles of FKBPL and CKAP4 in ER-phagy induction, we introduced various stress-inducing reagents, including ER stress inducers (A23187, DTT, and TM), an mTOR inhibitor (rapamycin), and nutrient starvation (EBSS). Interestingly, EBSS was the most effective at inducing ER-phagy, followed by rapamycin, with TM being less effective. Conversely, A23187 and DTT reduced ER-phagic flux compared to untreated controls (Fig. 5a–f). In addition, the absence of FKBPL and/or CKAP4 diminished ER-phagic flux under these stress-inducing conditions (Fig. 5a–f), highlighting that both FKBPL and CKAP4 are necessary for effective ER-phagy induction.

Since CKAP4 is a linear transmembrane protein with limited membrane curvature capabilities⁴⁰, we investigated how the FKBPL-CKAP4 axis induces ER fragmentation and ER-phagy. Based on the predicted structure of FKBPL and its self-association properties, we hypothesized that FKBPL might play a role in generating membrane curvature. To explore this, we employed two different biotinylation strategies (Fig. 5g). The first strategy used biotin ligase APEX, which allows for the detection of protein-protein interactions at specific time points. This technique involves converting biotin-phenol into short-lived radicals in the presence of H_2O_2 , which then rapidly labels nearby substrates⁴⁷. Pull-down assays with streptavidin-agarose revealed that at the 1.5 h time point, only EBSS treatment showed an interaction between FKBPL and CKAP4 (Fig. 5h). At the 2.5 h time point, FKBPL self-association was notably increased in cells treated with TM, rapamycin, or EBSS, correlating with the results from previous ER-phagic flux assessments. In contrast, the FKBPL-CKAP4 interaction was enhanced in A23187- and rapamycin-treated cells, but not in DTT-, TM-, and EBSS-treated cells (Fig. 4i).

We also employed another biotin ligase, TurboID, which provides a longer time window for detecting protein-protein interactions by labeling nearby substrates⁴⁷. To investigate the interaction between FKBPL and CKAP4, we used split-TurboID-FKBPL constructs, which included 1–72 a.a. and 73–319 a.a. of TurboID fused to FKBPL (V5-TurboID(N)-FKBPL and V5-TurboID(C)-FKBPL)⁴⁷. Pull-down assays revealed that between 1 to 2 h, only EBSS promoted the dimerization of FKBPL with CKAP4 and facilitated FKBPL oligomerization (Fig. 5j). From 2 to 3 h, TM increased the interaction between FKBPL dimers and CKAP4, as well as FKBPL oligomerization. In contrast, A23187 enhanced FKBPL oligomerization but did not support dimeric FKBPL binding to CKAP4. DTT inhibited both FKBPL dimer-CKAP4 interaction and FKBPL oligomerization. Rapamycin and EBSS showed a slight increase in FKBPL dimer-CKAP4 interaction but a decrease in FKBPL oligomerization (Fig. 5k). The reduction in FKBPL dimer-CKAP4

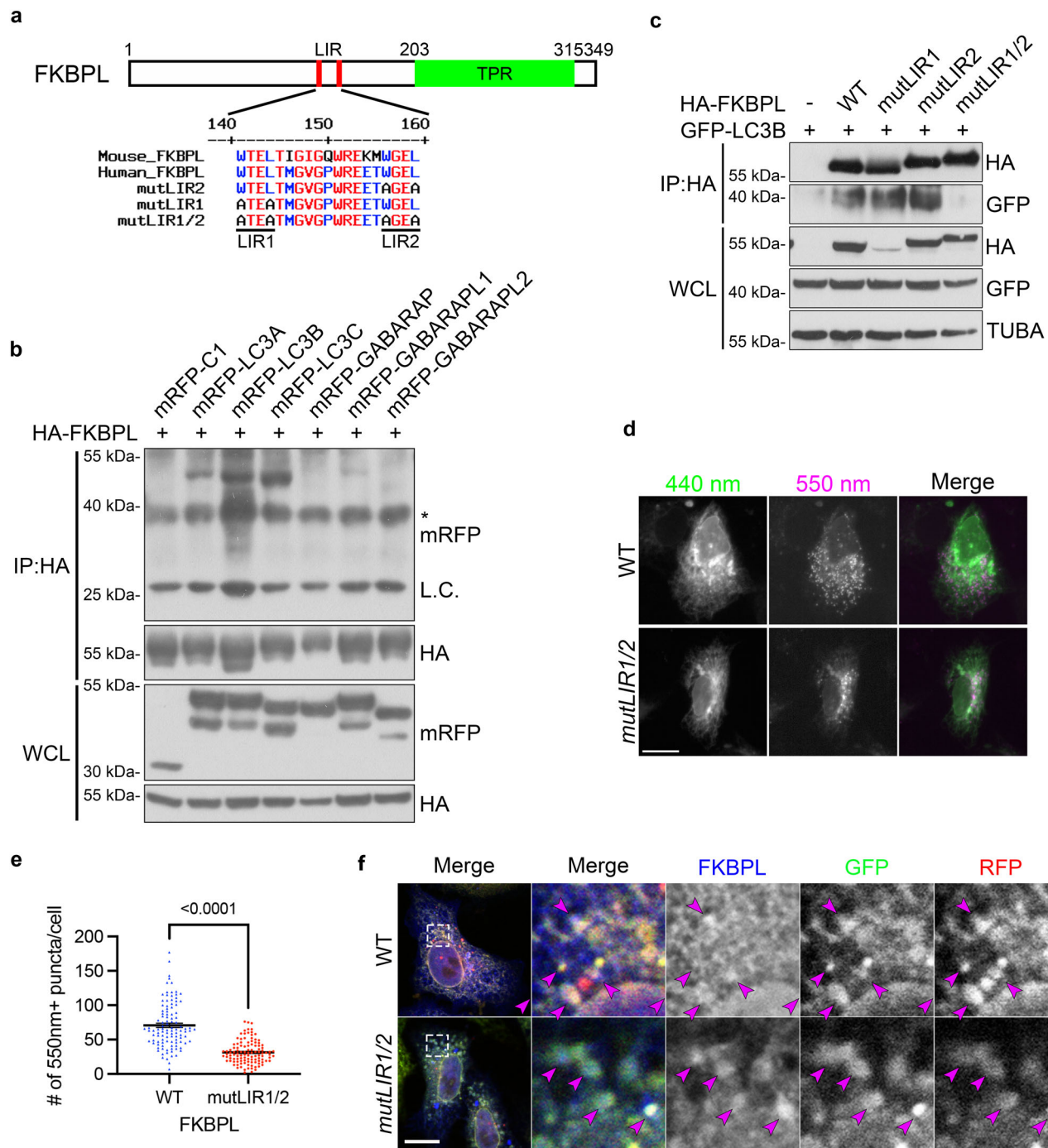
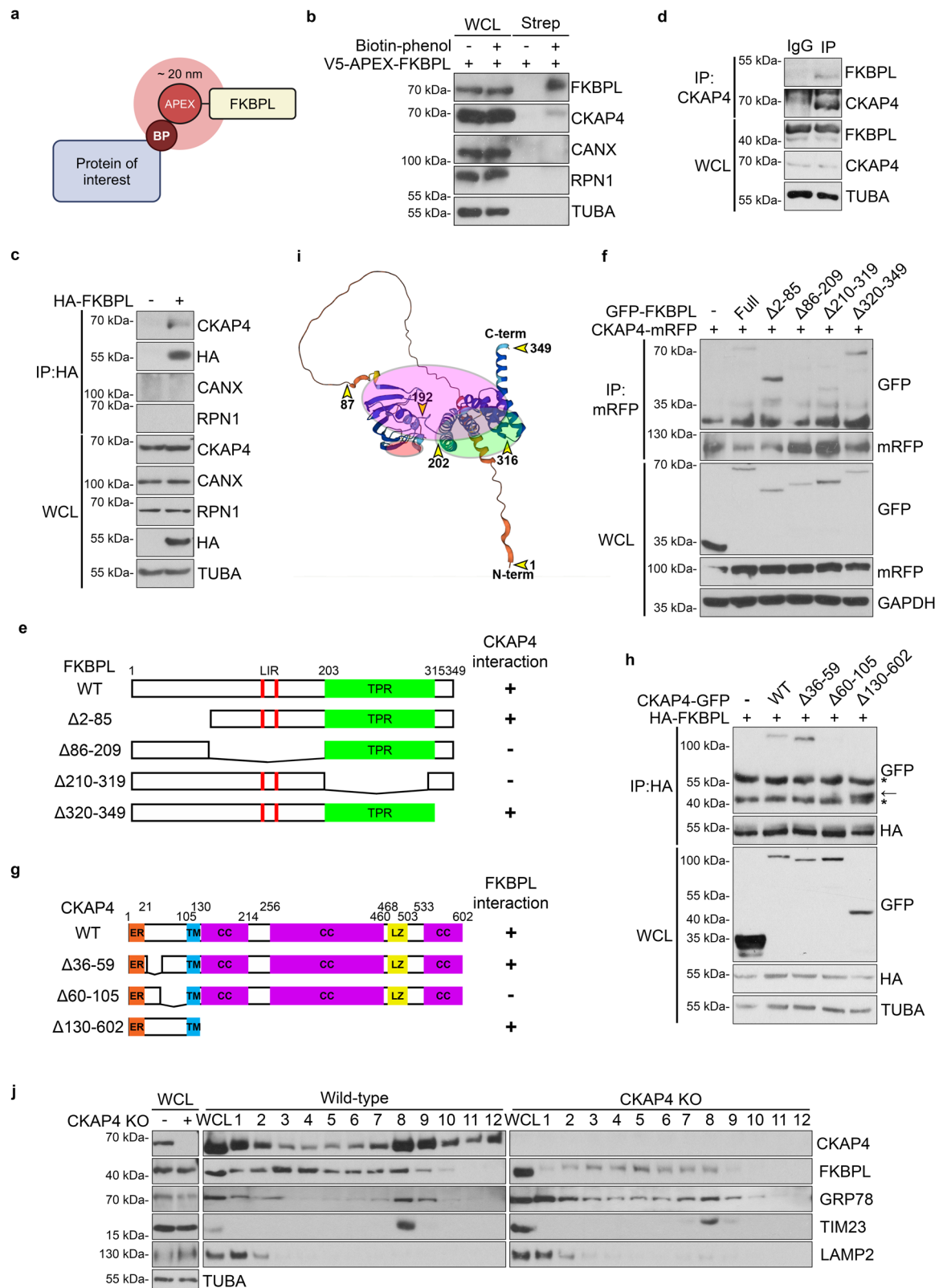


Fig. 2 | FKBPL interacts with LC3/GABARAP via two LIR motifs. **a** Domain architecture of FKBPL and alignment of the LIR motifs and their mutants (mutLIR). Red, LC3-interacting region (LIR); Green, tetratricopeptide (TPR). Numbers indicate amino acid residues of human FKBPL. **b** HEK293T cells were co-transfected with HA-FKBPL and mRFP-C1 or mRFP-tagged LC3/GABARAP. Immunoprecipitates of anti-HA antibody and whole cell lysates (WCL) were analyzed by immunoblotting. **c** HEK293T cells were co-transfected with GFP-LC3B and pcDNA-HA (-) or the indicated HA-FKBPL constructs. Immunoprecipitates of anti-HA antibody and WCL were

analyzed by immunoblotting. **d**, **e** Hep3B cells were co-transfected with mKeima-SEC61B and FKBPL WT or mutLIR1/2 and observed by fluorescence microscope (**d**). Numbers of 440 nm⁺/550 nm⁺ puncta were quantified. Data represent the mean ± SEM of three independent experiments. Differences were statistically analyzed by a two-tailed *t* test (**e**). **f** HeLa/ssRFP-EGFP-KDEL cells were transfected with FKBPL WT or mutLIR1/2. After 16 h, cells were maintained in full medium containing 1 µg/ml doxycycline for another 16 h, fixed, immunostained with anti-HA antibody, and observed by confocal microscope. Scale bars in (**d**) and (**f**) are 10 µm.

interaction and FKBPL oligomerization observed with rapamycin and EBSS might be attributed to lysosomal degradation occurring between 2 to 3 h. Overall, these findings suggest EBSS initiates ER-phagy by first facilitating the interaction between FKBPL and CKAP4, followed by FKBPL oligomerization. TM induces these changes more slowly, while rapamycin produces intermediate effects. A23187 does not effectively

induce ER-phagy because FKBPL-CKAP4 interaction and FKBPL oligomerization occur independently. DTT prevents ER-phagy by disrupting both FKBPL-CKAP4 interaction and FKBPL oligomerization. These data collectively indicate that stress conditions inducing ER-phagy facilitate FKBPL-CKAP4 interaction, which is subsequently followed by FKBPL oligomerization (Fig. 5I).



FKBPL-CKAP4 deficiency enhances protein secretion via microvesicle shedding and secretory autophagy

Unexpectedly, we observed that RFP and GFP fluorescence intensities were reduced in HeLa/ssRFP-EGFP-KDEL/FKBPL-CKAP4 double knockout (DKO) cells following doxycycline withdrawal. Although the levels of full-length ssRFP-EGFP-KDEL remained similar among WT, FKBPL KO, CKAP4 KO, and DKO cells while doxycycline was

present, they were significantly lower in DKO cells at 24 h after doxycycline withdrawal (Fig. 6a, b). This decrease occurred despite the reduced ER-phagic flux observed in DKO cells (Fig. 6c–e). Notably, this reduction could not be reversed by inhibiting lysosomal (Baf. A1) or proteasomal (MG132) activity (Supplementary Fig. S11). We then investigated whether the reporter protein was being secreted into the extracellular space. Prolonged doxycycline

Fig. 3 | CKAP4 is the ER-resident receptor for FKBPL. **a** Schematic representation of V5-APEX-FKBPL assay: V5-APEX-FKBPL biotinylates protein of interest ~ 20 nm nearby. The illustration created with BioRender.com is released under a Creative Commons Attribution-NonCommercial-NoDerivs 4.0 International license <https://creativecommons.org/licenses/by-nc-nd/4.0/deed.en>. **b** HEK293T cells were transfected with V5-APEX-FKBPL, left treated or untreated with biotin-phenol for 30 min, and then biotinylated in the presence of H₂O₂ for 1 min. Biotinylated proteins pulled down by Streptavidin-Agarose and WCL were analyzed by immunoblotting. **c** HEK293T cells were transfected with HA-FKBPL. Immunoprecipitates of anti-HA antibody and WCL were analyzed by immunoblotting. **d** Immunoprecipitates of anti-CKAP4 antibody and WCL of HEK293T cells were analyzed by immunoblotting. **e** Domain mapping of FKBPL binding to CKAP4. FKBPL WT and deletion mutants (left). The interaction between CKAP4-mRFP and GFP-FKBPL is noted. +, interaction; -, no interaction (right). **f** HEK293T cells were co-transfected with CKAP4-mRFP and EGFP-C1 (-) or the indicated GFP-FKBPL

constructs. Immunoprecipitates of anti-mRFP antibody and WCL were analyzed by immunoblotting. **g** Domain mapping of CKAP4 binding to FKBPL. CKAP4 WT and deletion mutants (left). The interaction between HA-FKBPL and CKAP4-mRFP is noted. +, interaction; -, no interaction (right). **h** HEK293T cells were co-transfected with HA-FKBPL and EGFP-N1 (-) or the indicated CKAP4-GFP constructs. Immunoprecipitates of anti-HA antibody and WCL were analyzed by immunoblotting. Arrow, CKAP4 deletion (Δ 130-602); asterisk, non-specific. **i** Protein structure of human FKBPL predicted by AlphaFold. Representing amino acid numbers are indicated. The magenta oval covers the CKAP4-interacting region (amino acids 86–202); the Red oval covers LIR motifs (₁₄₁WTEL₁₄₄ and ₁₅₆WGEL₁₅₉); the Green oval covers FKBPL self-interacting region (amino acids 203–315). **j** Membrane fractionation with continuous iodixanol gradient was performed using cell extract of HeLa/WT or CKAP4 KO cells. WCL and 12 fractions collected from lighter to heavier ones (Fractions 1 to 12) were analyzed by immunoblotting.

withdrawal led to higher levels of full-length ssRFP-EGFP-KDEL in the conditioned medium (CM) of DKO cells and lower levels in cell extracts (CELL) compared to WT cells (Fig. 6f–i). In contrast, the cellular and extracellular levels of reporter proteins were unaffected by TEX264 KO or FIP200 KO (Fig. 6f–i). Thus, the increased secretion of the ER-resident reporter proteins in FKBPL-CKAP4 DKO cells suggests enhanced protein secretion. Further investigation in HeLa/FKBPL-CKAP4 DKO cells revealed that the levels of two secretory proteins, COL1A2 and serpin family A member 1 (SERPINA1), were significantly higher in conditioned medium of DKO cells compared to WT cells (Fig. 6j–l). In addition, secretion of the cytosolic protein GAPDH was also increased in DKO cells (Fig. 6j, m). Importantly, there was no evidence of plasma membrane damage (Supplementary Fig. S12a–c) or increased cell death (Supplementary Fig. S12d–f) in DKO cells. Therefore, the absence of FKBPL and CKAP4 results in enhanced protein secretion.

Unexpectedly, we observed an accumulation of RFP-only puncta at the cell periphery following prolonged doxycycline withdrawal in HeLa/ssRFP-EGFP-KDEL FKBPL-CKAP4 DKO cells (Supplementary Fig. S13). A similar phenotype was observed in WT cells treated with brefeldin A (BFA), with severe accumulation of RFP-only puncta at the edges in DKO cells treated with BFA (Fig. 7a). BFA is known to cause Golgi disassembly⁴⁸, leading us to investigate whether there might be abnormal connections between Golgi disassembly, secretory vesicle formation, and protein secretion. Immunocytochemical analysis revealed that DKO cells exhibited a dispersed Golgi apparatus, similar to the Golgi disruption seen in BFA-treated WT cells (Supplementary Fig. S14). Although ER-phagic flux was suppressed in both DKO cells and BFA-treated WT cells, the secretion of ssRFP-EGFP-KDEL was enhanced in these conditions (Fig. 7b, c). These findings suggest that the deficiency of FKBPL and CKAP4 impacts Golgi integrity, which correlates with changes in protein secretion.

Since both ER-derived and cytosolic proteins are secreted in the absence of FKBPL and CKAP4, we also examined the distribution of cytosolic proteins in FKBPL-CKAP4 DKO cells. We observed that cytosolic GAPDH and SEC24C/D accumulated in the outward budding of the plasma membrane and remained detectable even after extracellular proteins were degraded with proteinase K (Supplementary Fig. S15), suggesting their intracellular localization. This plasma membrane budding is typical of microvesicle shedding. Activation of small GTPase ARF6 is crucial for the budding and pinching off of microvesicle²⁶. Treatment with the ARF6 inhibitor NAV2729 suppressed microvesicle shedding in DKO cells (Fig. 7d). Levels of the lysosomal membrane protein LAMP2 and the cytosolic protein GAPDH in conditioned medium were also reduced by NAV2729 (Fig. 7e). Intriguingly, cathepsin D levels decreased in DKO cells, indicating reduced lysosomal activity. This is consistent with previous reports showing that inhibition of lysosomal activity facilitates protein secretion via secretory autophagy²⁷.

EGFP loses its fluorescent signals in pH under 6.0⁴⁹, while the luminal pH of the trans-Golgi network and late endosomes is about 6.0, and secretory vesicles are about 5.5⁵⁰. In the EGFP-RFP-KDEL assay in DKO cells, the accumulation of RFP-only puncta at the peripheral region indicates increased acidity of ER-derived vesicles (Fig. 7a). To dissect the roles of autophagy and lysosomal activity in protein secretion, we measured the secretion of ssRFP-EGFP-KDEL. We found that lysosome inhibition by Baf. A1 triggered protein secretion in WT cells similar to untreated DKO cells (Fig. 7f). Together with the decreased levels of cathepsin D in DKO cells (Fig. 7e), these results indicate that lysosomal activity is reduced in DKO cells. Conversely, treatment with NAV2729 and inhibition of autophagy by 3-methyladenine (3-MA) or wortmannin blocked the secretion of ssRFP-EGFP-KDEL in DKO cells (Fig. 7e), suggesting that autophagy machinery is also required for protein secretion, in addition to microvesicle shedding, in DKO cells. Furthermore, we found that proteasome inhibitor MG132 attenuated the secretion of ssRFP-EGFP-KDEL in DKO cells (Fig. 7f). As proteasome inhibition can reciprocally regulate lysosome activity^{51,52}, we examined lysosomal activity using DQ-Red-BSA, which exposes its red fluorescent dyes upon lysosomal degradation of BSA⁵³. We found that MG132 slightly increased lysosomal acidity in both WT and DKO cells (Fig. 7g). Although NAV2729-suppressed protein secretion in DKO cells, it failed to restore lysosomal activity and even decreased it in WT cells (Fig. 7g), suggesting that microvesicle shedding is the immediate cause of protein secretion in FKBPL-CKAP4-deficient cells. Together, FKBPL-CKAP4 deficiency leads to multiple alterations, including Golgi and lysosome impairment and enhanced protein secretion, which is mediated by microvesicle shedding.

Discussion

In this study, we show that FKBPL, with the aid of CKAP4, mediates both ER fragmentation and ER-phagy. ER-phagy-inducing conditions trigger FKBPL-CKAP4 interaction followed by FKBPL oligomerization at the ER, while FKBPL-CKAP4 deficiency leads to protein secretion via microvesicle shedding (Fig. 8).

Although many ER-resident membrane proteins have been identified as ER-phagy receptors, CKAP4 itself does not act as an ER-phagy receptor due to the lack of an LIR motif. Unlike FAM134B and RTN3L^{14,16}, which are known for their roles in ER-phagy and have the ability to induce membrane curvature, CKAP4 is predicted to have a linear protein structure and lacks membrane curvature ability. According to the AlphaFold database, FKBPL has a conserved N-terminal unstructured region and a curved structure across species. We believe that the predicted curved structure and self-interaction ability of FKBPL is key to its function in generating membrane curvature. Structure modeling and our results support this hypothesis: deletion of the N-terminal unstructured region in FKBPL increases the FKBPL-CKAP4 interaction, and CKAP4 appears to bind to FKBPL through the concave of the curved

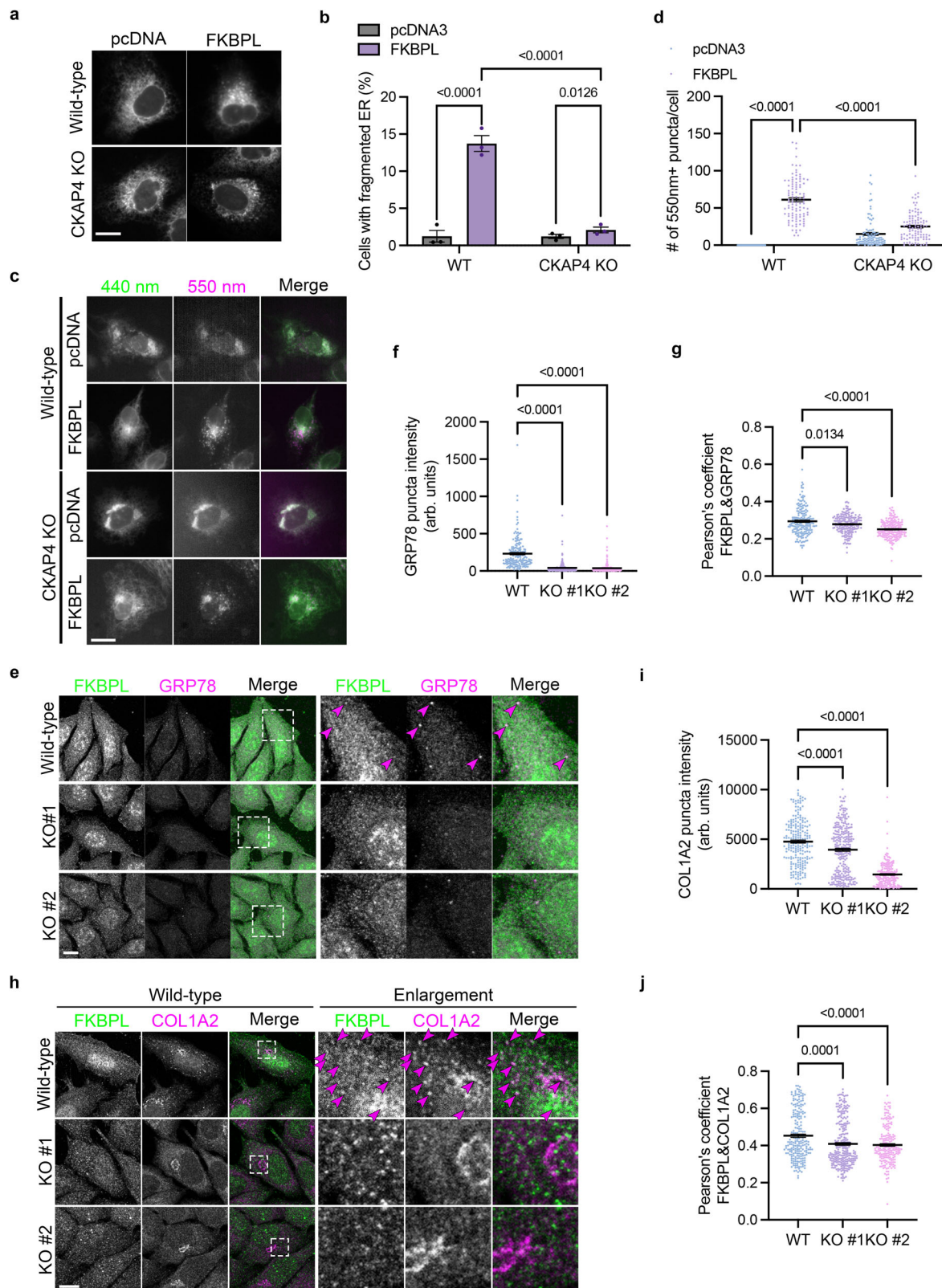
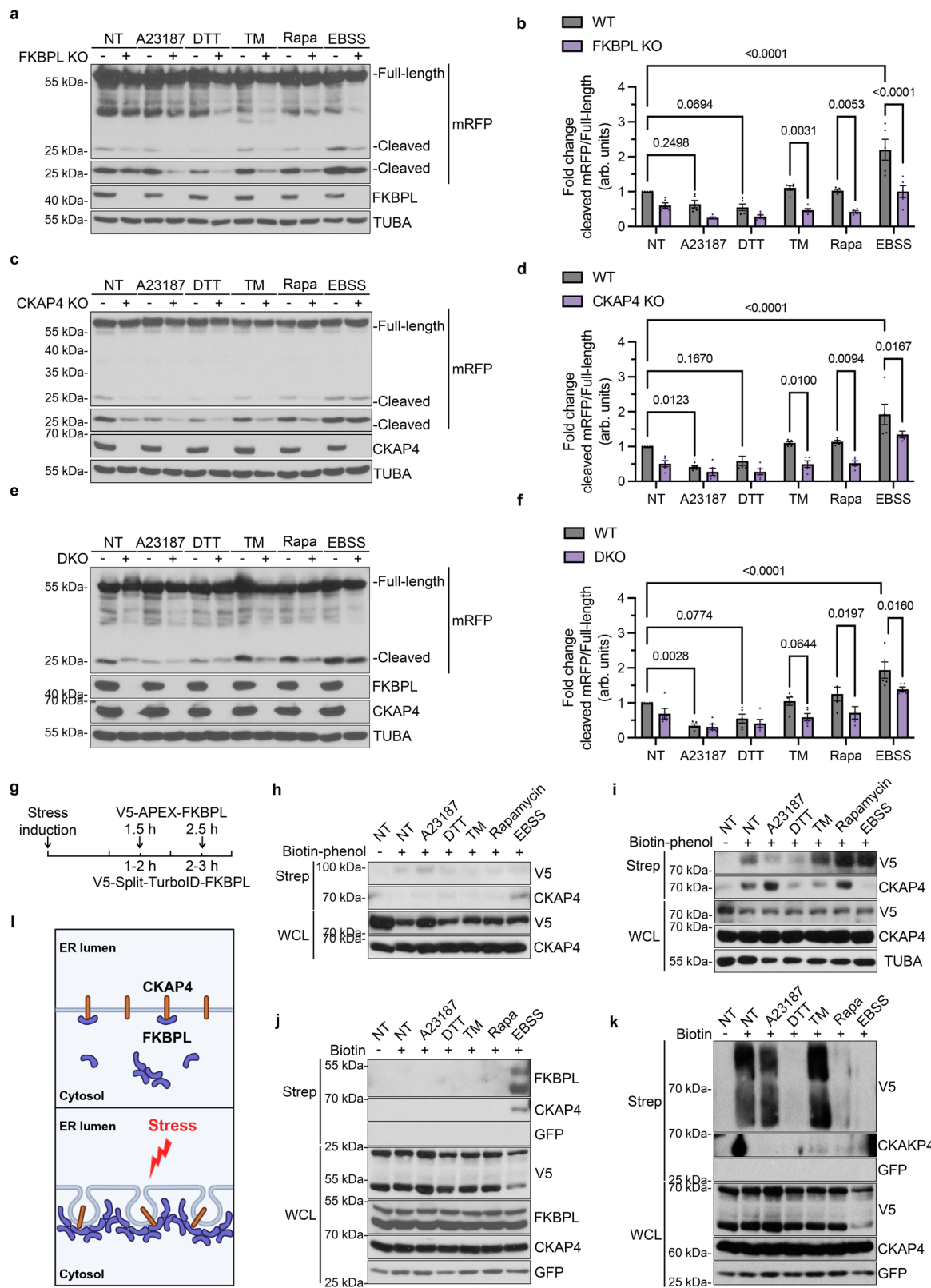


Fig. 4 | CKAP4 links FKBPL and ER luminal cargoes. **a** Hep3B/WT or CKAP4 KO cells were co-transfected with RFP-KDEL and pcDNA3.0 or FKBPL and observed by fluorescence microscope. **b** Ratio in cells with fragmented ER were quantified. **c, d** Hep3B/WT or CKAP4 KO cells co-transfected with mKeima-SEC61B, and either pcDNA3.0 or FKBPL were observed by fluorescence microscope (**c**). Numbers of 440 nm⁺/550 nm⁺ puncta were quantified (**d**). **e, h** HeLa/WT or CKAP4 KO cells were left untreated or treated with 2 μ g/ml tunicamycin (TM) together with 20 nM bafilomycin A1 (Baf. A1) for 6 h. Cells were fixed, immunostained with anti-FKBPL

and anti-GRP78 (**e**) or anti-COL1A2 (**h**) antibodies and observed by confocal microscope. **f, i** Puncta intensities of GRP78 (**f**) or COL1A2 (**i**) were analyzed by ImageJ BIOP JACoP. **g, j** Pearson's correlation coefficient of FKBPL and GRP78 (**g**) or COL1A2 (**j**) were analyzed using ImageJ BIOP JACoP. Scale bars in (**a, c, e, and h**) are 10 μ m. Data represent the mean \pm SEM of three independent experiments in (**b, d, f, g, i, and j**). Differences were statistically analyzed by one-way ANOVA followed by Dunnett's multiple comparisons test in (**b, d, f, g, i, and j**). Arbitrary units, arb. units.



structure in the middle. Although the LIR motifs (amino acids 141–144 and 156–159) and TPR domain (amino acids 210–319) of FKBPL overlap with CKAP4-binding domain (amino acids 86–319), the binding modules of FKBPL for LC3/GABARAP (LIR motifs) or FKBPL self-interaction (TPR domain) are predicted to be situated on the opposite side from that of CKAP4. Due to its structural flexibility, the unstructured region of FKBPL seems to act as a gatekeeper for CKAP4 entry.

Both FKBPL-CKAP4 interaction and FKBPL self-association are facilitated during ER-phagy under stress-induced conditions. Through various protein-protein interaction assays utilizing both endogenous and overexpressed recombinant proteins, we have demonstrated that ER-phagy-inducing stressors initially promote the interaction between FKBPL and CKAP4, followed by the oligomerization of FKBPL oligomerization at the ER. FKBPL

Fig. 5 | FKBPL-CKAP4 interaction and FKBPL oligomerization facilitate stress-induced ER-phagy. **a, c, e** HeLa/ssRFP-EGFP-KDEL WT, FKBPL KO (**a**), CKAP4 KO (**c**), and FKBPL-CKAP4 DKO (**e**) cells were incubated in full medium containing 1 μ g/ml doxycycline for 14 h. After briefly washed with PBS, cells were left untreated or treated with 1 μ M A23187, 0.5 mM dithiothreitol (DTT), 2 μ g/ml tunicamycin (TM), 100 nM rapamycin (Rapa), or EBSS for another 6 h. Cell extracts were analyzed by immunoblotting. **b, d, f** Signal intensities of the cleaved relative to full-length ssRFP-EGFP-KDEL were quantified. **g** Schematic representation of biotinylation assays using V5-APEX-FKBPL or V5-split-TurboID-FKBPL. **h, i** HEK293T cells were transfected with V5-APEX-FKBPL for 24 h and left untreated or treated with 1 μ M A23187, 0.5 mM DTT, 2 μ g/ml TM, 100 nM rapamycin (Rapa), or EBSS for 1 h (**h**) or 2 h (**i**). Cells were treated with 500 μ M biotin-phenol for another 30 min at 37 °C. Then, cells were incubated with 1 mM H₂O₂ for 1 min and quickly quenched with 5 mM

Trolox, 10 mM sodium azide, and 10 mM sodium ascorbate. **j, k** HEK293T cells were co-transfected with V5-TurboID(N)-FKBPL and V5-TurboID(C)-FKBPL (represented as V5-split-TurboID-FKBPL) for 24 h and left untreated or treated with 1 μ M A23187, 0.5 mM DTT, 2 μ g/ml TM, 100 nM Rapa, or EBSS for 1 h (**j**) or 2 h (**k**). Cells were treated with 100 mM biotin for another 1 h. Biotinylated proteins pulled down by Streptavidin-Agarose and whole cell lysates (WCL) were analyzed by immunoblotting. **l** Schematic representation of FKBPL-CKAP4-dependent ER-phagy induction under stress conditions. The illustration created with BioRender.com is released under a Creative Commons Attribution-NonCommercial-NoDerivs 4.0 International license <https://creativecommons.org/licenses/by-nc-nd/4.0/deed.en>. Data represents the mean \pm SEM of three independent experiments in (**b, d, and f**). Differences were statistically analyzed by one-way ANOVA followed by Dunnett's multiple comparisons test in (**b, d, and f**). Arbitrary units, arb. units.

oligomerization following its interaction with CKAP4 at the ER induces ER-phagy, rather than the independent occurrence of either FKBPL-CKAP4 interaction or FKBPL oligomerization. However, the precise mechanisms by which ER-phagy-inducing stressors enhance FKBPL-CKAP4 interaction and/or FKBPL oligomerization at the ER remain unclear. Potential post-translationally modification of FKBPL and CKAP4, or changes in FKBPL trafficking through cytoskeleton mediated by other regulators, needs to be elucidated. Furthermore, while the deletion of FKBPL and/or CKAP4 suppresses ER-phagic flux, it does not completely inhibit it. This suggests that other ER-phagy regulators are also involved in the execution of ER-phagy. Therefore, an important question remains, how do distinct ER-phagy receptors, including the FKBPL-CKAP4 axis, function, and to what extent are they engaged under specific stress conditions. This aspect requires further investigation to fully understand the complexity and regulation of ER-phagy.

Intriguingly, we found that a deficiency in the FKBPL-CKAP4 axis enhances both ER-derived and cytosolic protein secretion regardless of ER-phagy attenuation. FKBPL-CKAP4-deficient cells exhibit multiple alterations, including impairments in both the Golgi apparatus and lysosome. FKBPL-CKAP4 DKO cells show a distributed Golgi apparatus similar to that observed in BFA-treated cells, and both conditions enhance protein secretion. FKBPL-CKAP4 deficiency also leads to a decrease in lysosomal activity, while lysosomal inhibitor facilitates protein secretion. In addition, blocking the autophagy machinery with 3-MA or wortmannin reduces protein secretion. Since FKBPL-CKAP4-deficient cells show outward growth of the plasma membrane resembling microvesicle shedding, blocking microvesicle shedding by NAV2729 efficiently suppresses protein secretion as well as lysosomal activity. Although the manipulation of autophagosome formation and lysosomal activity seems to be related to protein secretion, direct evidence is still missing. While alterations in Golgi apparatus assembly, lysosome impairment, and plasma membrane shedding occur in FKBPL-CKAP4-deficient cells, a comprehensive understanding of protein secretion in these cells still needs to be elucidated.

In summary, this study presents the dual role of the FKBPL-CKAP4 axis in ER-phagy and protein secretion (Fig. 8). These findings highlight the complexity of the FKBPL-CKAP4 axis and its critical role in maintaining cellular homeostasis under stress conditions. A deeper understanding of how the FKBPL-CKAP4 axis influences these processes could provide new insights into therapeutic strategies for diseases related to ER stress and abnormal protein secretion.

Methods

Cell culture

HEK293T and HeLa cells were routinely maintained in DMEM/high glucose medium (HyClone) supplemented with 10% fetal bovine serum (FBS) (Gibco) and 100 μ g/ml penicillin-streptomycin (Gibco). Hep3B cells were maintained in RPMI-1640 (HyClone) supplemented with 10% FBS (Gibco) and 100 μ g/ml penicillin-streptomycin (Gibco).

Plasmid construction

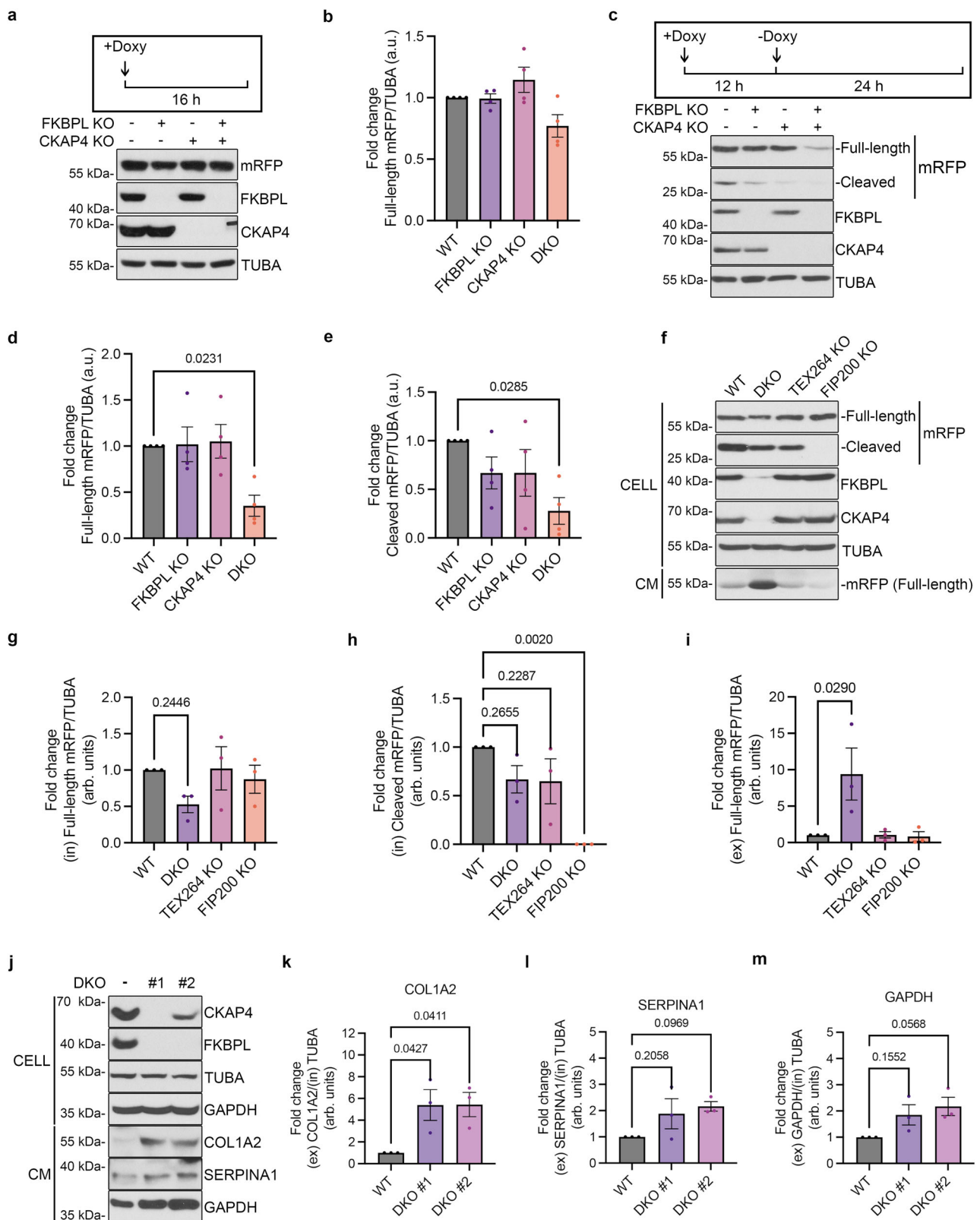
Human FKBPL and SEC61B were generated using the Gateway cloning system. Human CKAP4 was purchased from KRIBB, and FLAG-tagged constructs in Supplementary Fig. S10 were purchased from GeneCopoeia. FKBPL, CKAP4, and SEC61B were amplified by PCR, and the PCR products were subcloned into pcDNA3.0-HA, EGFP-C1, EGFP-N1, mRFP-C1, or mRFP-N1. mKeima was amplified and exchanged with GFP in GFP-SEC61B. V5-APEX or V5-TurboID were amplified and exchanged with GFP in GFP-FKBPL. Point mutants and deletion mutants of FKBPL or CKAP4 were generated by PCR-based site-directed mutagenesis. All cDNA constructs were confirmed by DNA sequencing analysis. The sgFKBPL and sgCKAP4 were inserted into Lentivector V2. The target sequence of sgFKBPL #1 is 5'-AGCTCAAGCGTTTGCCTAGGAGG; target sequence of sgFKBPL #2 is 5'-TTCGGATCAGGGCCGCCAGAGGG; target sequence of sgCKAP4 #1 is 5'-ACGTCATCCGCGCCGCCGACGG; target sequence of sgCKAP4 #2 is 5'-CTACACCGAGGTCCGCGA GCTGG.

Antibodies

Antibodies against FKBPL (63389-1-Ig; 10060-1-AP) and CKAP4 were purchased from Proteintech; antibody against FLAG M2 (F3165) and FLAG M2 affinity gel (A2220) were purchased from Sigma-Aldrich; antibodies against GAPDH (sc-47724), GFP (sc-9996), GRP78 (sc376768), HA (sc-7392), RPN1 (sc-48367), TUBA (sc-23948), CANX (sc-11397), CTSD (sc-6486) were purchased from Santa Cruz Biotechnology; antibodies against GM130 (610822), TIM23 (611222) were purchased from BD Biosciences; antibody against KDEL (ADI-SPA-827-F) was purchased from Enzo Life Sciences; antibody against UB (MAB1510) was purchased from Chemicon; antibody against V5 (ab27671) was purchased from Abcam; antibodies against LAMP2A (NBP2-22217) and LC3B (NB100-2220) were purchased from Novus Biologicals; antibody against Caspase 3 (9662 P) was purchased from Cell Signaling Technology; antibodies against GAPDH (A19056), COL1A2 (A8335), LMNA1 (A10440), SEC24C (A10797), SEC24D (A16091), SERPINA1 (A12481) were purchased from ABclonal; antibody against HSP90a (GTX109753) was purchased from GeneTex; antibody against Golgin-97 was purchased from Invitrogen. HRP-conjugated goat anti-mouse secondary antibody (31430), HRP-conjugated goat anti-rabbit secondary antibody (31460), HRP-conjugated rabbit anti-goat antibody (31402), goat anti-mouse secondary antibody Alexa 405 (A48255), goat anti-mouse secondary antibody Alexa 488 (A11001), goat anti-mouse secondary antibody Alexa 594 (A11005), goat anti-rabbit secondary antibody Alexa 488 (A11008), goat anti-rabbit secondary antibody Alexa 594 (A11012), streptavidin Alexa 568 (S11226) were purchased from Thermo Fisher Scientific. Protein G Sepharose 4 Fast Flow (17-0618-05) was purchased from GE Healthcare. Streptavidin-Agarose (16-126) was purchased from Millipore.

Chemicals and reagents

3-Methyladenine (M9281), A23187(C7522), Acridine orange (A6014), biotin (B4501), biotin-phenol/biotinyl tyramide (SML2135), brefeldin A



(B7651), dimethyl sulfoxide (D2650), doxycycline (D23447), fluoromount aqueous mounting medium (F4680), hydrogen peroxide solution (H1009), Opti-Prep density gradient medium (D1556), phenylmethylsulfonyl fluoride (P7626), polybrene (H9268), polyethylenimine (408727), propidium iodide (P4170), tunicamycin (T7765), wortmannin (W1628) were purchased from Sigma-Aldrich; albumin (A0100-010) was purchased from GenDEPOT; bafilomycin A1

(196000) was purchased from Calbiochem; Bio-Rad protein assay dye reagent concentrate (500-0006) was purchased from BIO-RAD; Calcein, AM (C1430), DQ-Red-BSA (D12051), ER-Tracker Blue-White DPX (E12353) were purchased from Invitrogen; dithiothreitol (DTT10) was purchased from GoldBio; ethidium bromide (1239-45-8) was purchased from USB; Hoechst 33342 (62249), Lipofectamine 2000 were purchased from Thermo Fisher Scientific; Lipofector pMAX

Fig. 6 | Loss of FKBPL and CKAP4 facilitates protein secretion. a, b HeLa/ssRFP-EGFP-KDEL WT, FKBPL KO, CKAP4 KO, and FKBPL-CKAP4 DKO cells were incubated in full medium containing 1 μ g/ml doxycycline for 16 h and analyzed by immunoblotting (a). Signal intensities of full-length ssRFP-EGFP-KDEL relative to TUBA were quantified (b). **c–e** HeLa/ssRFP-EGFP-KDEL WT, FKBPL KO, CKAP4 KO, and FKBPL-CKAP4 DKO cells were incubated in full medium containing 1 μ g/ml doxycycline for 12 h, doxycycline-free medium for another 24 h, and analyzed by immunoblotting (c). Signal intensities of full-length ssRFP-EGFP-KDEL (d) and cleaved ssRFP-EGFP-KDEL (e) relative to TUBA were quantified. **f–i** HeLa/ssRFP-EGFP-KDEL WT, FKBPL-CKAP4 DKO, TEX264 KO, and FIP200 KO cells were incubated in full medium containing 1 μ g/ml

doxycycline for 12 h, doxycycline-free medium for another 24 h, and cell extracts (CELL) and conditioned medium (CM) were analyzed by immunoblotting (f). Signal intensities of full-length ssRFP-EGFP-KDEL (g) and the cleaved ssRFP (h) in cell extracts (CELL), and ssRFP-EGFP-KDEL (i) in CM relative to TUBA were quantified. **j–m** Cell extracts (CELL) and CM of HeLa/WT and FKBPL-CKAP4 DKO were analyzed by immunoblotting (j). Signal intensities of COL1A2 (k), SERPINA1 (l), and GAPDH (m) in CM relative to TUBA were quantified. Data represents the mean \pm SEM of four independent experiments in (b, d, e) and four independent experiments in (g–i, k, l, and m). Differences were statistically analyzed by one-way ANOVA followed by Dunnett's multiple comparisons test in (b, d, e, g, h, i, k, l, and m). Arbitrary units, arb. units.

(AB-LF-M100) was purchased from AptaBio; MG132 (BML-PO102-0025) was purchased from Enzo Life Sciences; NAV2729 (5986) was purchased from Tocris Bioscience; protease inhibitor cocktail (PPI015) was purchased from Quartett.

DNA transfection

HEK293T cells were transfected with polyethylenimine (PEI) (Sigma-Aldrich), and HeLa and Hep3B cells were transfected with Lipofectamine 2000 (ThermoFisher) or Lipofector pMax (AptaBio) according to the manufacturer's instruction.

Gain-of-function screen and assessment of cells with ER fragmentation

Among ~2000 ER-resident proteins categorized in the NCBI, 442 candidates with potential LIR motifs were selected based on amino acid sequence using the prediction program iLIR, hfAIM. Among those 442 candidates, 135 cDNAs encoding potential ER-phagy receptor candidates were collected. Hep3B cells were co-transfected with ER marker RFP-KDEL and each candidate cDNA in mammalian expression vector by a ratio of 1:9 using Lipofector pMax reagent (AptaBio). After 24 h, ER morphology was observed under a fluorescent microscope Olympus IX71. The pcDNA3.0 and FAM134B were used as negative and positive controls, respectively.

Assessment of ER-phagic flux with mKeima-SEC61B

Hep3B cells were transfected with FKBPL and mKeima-SEC61B by a ratio of 9:1. After 24 h, 440 nm exited signal, and 550 nm exited signal were captured by fluorescence microscope Olympus IX71. 440 nm⁺/550 nm⁺ round puncta were counted, representing mKeima-SEC61B in acidic vesicles pH lower than 5.5.

Generation of knockout cell lines using CRISPR-Cas9 systems

A sgRNA targeting FKBPL or CKAP4 was introduced into the Lenti-vector V2 carrying Cas9 enzyme. The resulting sgFKBPL and sgCKAP4 lentivector were transfected into HEK293T cells together with the packaging plasmid psPAX2 and envelope plasmid pCMV-VSV-G (by a ratio of 5:3:2) using PEI. After 42 h, the supernatant containing lentiviruses was collected and treated for 24 h to host cells using 8 μ g/ml polybrene. Cells were then selected by incubating with 1 mg/ml puromycin for another 24 h, and single clones of selected cells were prepared by limited dilution and analyzed by western blotting.

Cell lysis and immunoblotting

Cells were lysed with RIPA buffer (50 mM Tris-Cl pH8.0, 150 mM NaCl, 1% NP-40, 0.5% sodium deoxycholate, 0.1% SDS) containing protease inhibitor cocktail (Quartett) and 1 mM PMSF, and cleared by centrifugation (12,000 \times g, 20 min, at 4 °C). Concentration of protein was measured with Bradford protein assay. The supernatant was sampled with 4X Laemmli buffer (250 mM Tris-Cl pH6.8, 10% SDS, 20% β -mercaptoethanol, 40% glycerol, 0.08% bromophenol blue) to 1X followed by 5 min boiling at 95 °C, separated by SDS-PAGE, and transferred to polyvinylidene difluoride (PVDF) membrane with semi-dry transfer system WSE-4025 HorizeBLOT 2M-R (ATTO). After blocked with 5% BSA (GenDEPOT), the membrane was incubated with primary antibody O/N

at 4 °C, washed with TBST three times for 10 min with agitation, and incubated with secondary antibody for 1 h at room temperature. Signals were visualized after the ECL reaction and exposed to X-ray film.

Immunoprecipitation

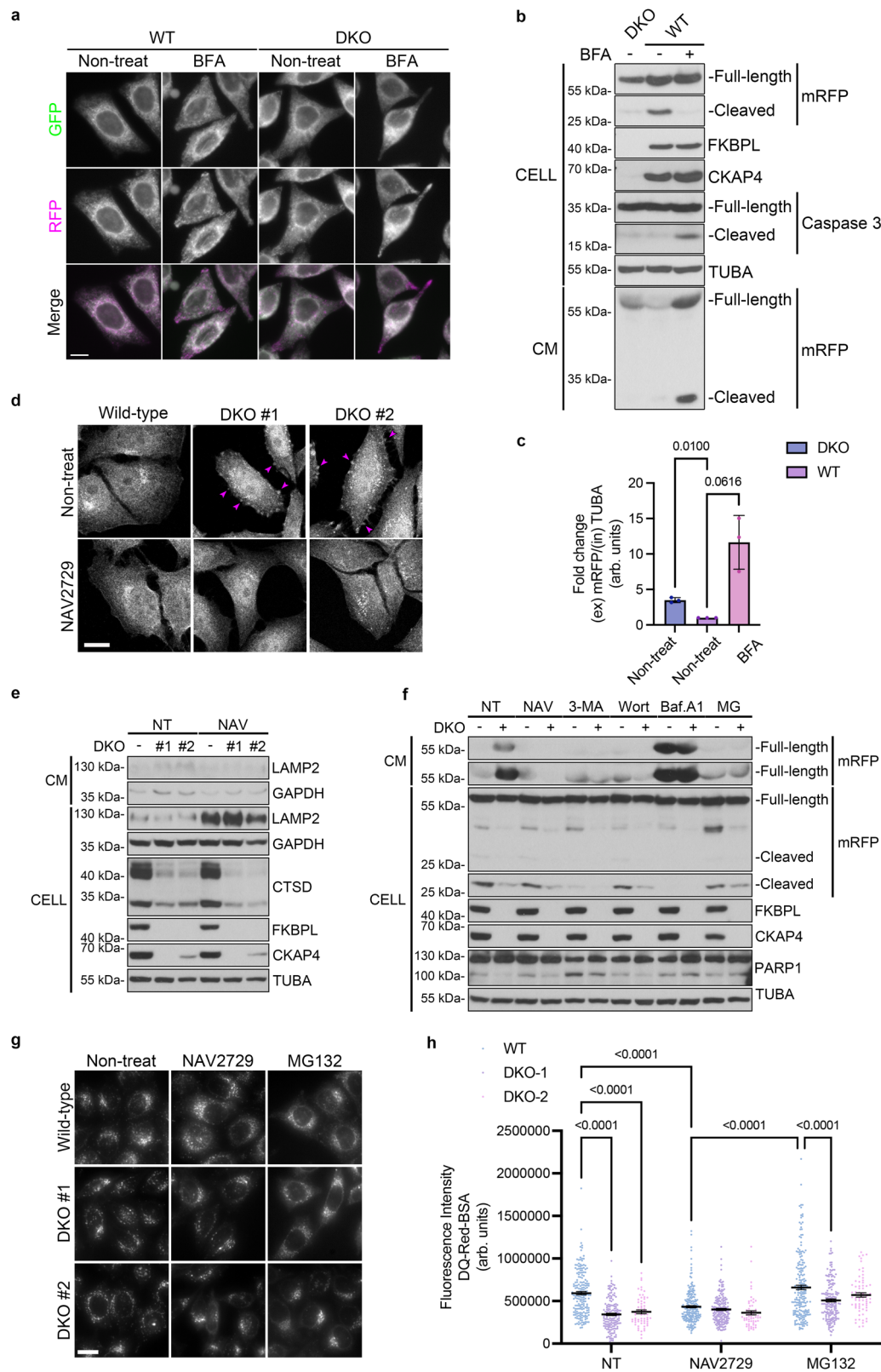
For overexpression immunoprecipitation, HEK293T cells were transfected with plasmids (by a ratio of 1:1) using PEI. After 24 h, cells were lysed with lysis buffer (50 mM Tris-Cl pH 7.4, 150 mM NaCl, 1 mM EDTA, 1% Triton X-100) containing protease inhibitor cocktail (Quartett) and 1 mM PMSF (Sigma-Aldrich), and cleared by centrifugation (12,000 \times g, 20 min, at 4 °C). Supernatant was transferred to a new tube and incubated with primary antibody in lysis buffer O/N at 4 °C. Protein G Sepharose bead slurry (GE Healthcare) or FLAG M2 bead slurry (Sigma-Aldrich) were added and incubated at 4 °C for 4 h. Beads were washed three times with lysis buffer, cleared by syringe, eluted with 1X sample buffer (46.7 mM Tris-Cl pH6.8, 5% glycerol, 1.67% SDS, 1.55% DTT, 0.02% bromophenol blue) followed by 5 min boiling at 95 °C, and analyzed by immunoblotting.

Biotinylation

The biotinylation assay was modified from the previous study³⁶. HEK293T cells were transfected with V5-APEX-FKBPL. After 24 h, cells were briefly washed with PBS and maintained in full media containing 1 μ M A23187, 0.5 mM DTT, 2 μ g/ml tunicamycin, 100 nM rapamycin, or EBSS for 1 or 2 h. Then, 500 μ M biotin-phenol (Sigma-Aldrich) was added and incubated for 30 min at 37 °C. 1 mM H₂O₂ was added for 1 min with gentle agitation and quenched by washing three times with PBS containing 5 mM Trolox (Sigma-Aldrich), 10 mM sodium azide (Sigma-Aldrich), and 10 mM sodium ascorbate (Sigma-Aldrich). V5-TurboID(N)-FKBPL (including 2–72 a.a. of TurboID) and V5-TurboID(C)-FKBPL (including 73–319 a.a. of TurboID) were generated by PCR-based site-directed mutagenesis. HEK293T cells were co-transfected with V5-TurboID(N)-FKBPL and V5-TurboID(C)-FKBPL. After 24 h, cells were briefly washed with PBS and maintained in full media containing 1 μ M A23187, 0.5 mM DTT, 2 μ g/ml tunicamycin, 100 nM rapamycin, or EBSS for 1 or 2 h. Then, 100 μ M biotin was added, incubated for 1 h at 37 °C, and briefly washed with PBS. HEK293T cells were lysed with RIPA buffer, sonicated, and cleared by centrifugation (12,000 \times g, 20 min, at 4 °C), and pull-downed using Streptavidin-Agarose bead slurry (EMD Millipore; 16–126) at 4 °C for 4 h. Beads were washed three times with RIPA buffer, cleared by syringe. Streptavidin pulled-down substrates eluted with 1X sample buffer (46.7 mM Tris-Cl pH 6.8, 5% glycerol, 1.67% SDS, 1.55% DTT, 0.02% bromophenol blue) in the presence of 2 mM biotin followed by 5 min boiling at 95 °C and WCL were analyzed by immunoblotting.

Identification of FKBPL-binding proteins by LC-MS/MS

Immunoprecipitates were separated by SDS-PAGE, and the gel was stained with Coomassie blue. Bands of interest on the gel were cut-out and excised. The excised gel slice was destained using 30% acetonitrile for 1 h. The proteins were denatured with 8 M urea in 50 mM ammonium bicarbonate, reduced with 20 mM DTT for 10 min, and then alkylated with 55 mM iodoacetamide for 1 h. After dilution to 1 M urea in 50 mM ammonium bicarbonate, proteins were digested with 0.5 μ g



trypsin O/N at 37 °C. Before mass spectrometry analysis, solid-phase extraction clean-up and sample concentration in speed-vac were preceded. Mass spectrometry was analyzed using Orbitrap Fusion Lumos Tribrid MS (Thermo Fisher Scientific) coupled with a nanoAcquity system (Waters) equipped with an in-house packed capillary analytical column (75 μ m x 100 cm) and trap column (159 μ m x 3 cm) with 3 μ m Jupiter C18 particles (Phenomenex). All datasets were searched using

Proteome Discoverer (Thermo Fisher Scientific) against the UniProt Human reference proteome database.

Immunocytochemistry

Cells were washed three times with PBS, fixed in 4% paraformaldehyde (Sigma-Aldrich) in PBS for 10 min, permeabilized with 0.5% saponin in PBS for 30 min, and blocked with 4% BSA in PBS-T for 1 h. Cells were

Fig. 7 | Microvesicle shedding is the immediate cause of protein secretion in FKBPL-CKAP4-deficient cells. **a** HeLa/ssRFP-EGFP-KDEL WT and FKBPL-CKAP4 DKO cells were incubated with 1 μ g/ml doxycycline for 16 h and then left untreated or treated with 5 μ g/ml brefeldin A (BFA) for another 6 h. Cells were fixed and observed by a confocal microscope. **b, c** HeLa/ssRFP-EGFP-KDEL WT and FKBPL-CKAP4 DKO cells were incubated with full medium containing 1 μ g/ml doxycycline for 16 h and then left untreated or treated with 50 ng/ml BFA for 24 h. Cell extracts (CELL) and CM were analyzed by immunoblotting (**b**). Signal intensities of full-length RFP-EGFP-KDEL in conditional medium (CM) relative to TUBA in cell extracts were quantified (**c**). **d** HeLa/FKBPL-CKAP4 DKO cells were left untreated or treated with 1 μ M NAV2729 for 24 h and fixed, permeabilized, immunostained with anti-GAPDH, and observed by confocal microscope. **e** Cell extracts and CM of HeLa/WT or FKBPL-CKAP4 DKO cells left untreated or treated with 1 μ M NAV2729 for 24 h

were analyzed by immunoblotting. **f** HeLa/ssRFP-EGFP-KDEL WT or FKBPL-CKAP4 DKO cells were incubated in full medium containing 1 μ g/ml doxycycline for 12 h, doxycycline-free medium containing 1 μ M NAV2729, 5 mM 3-methyladenine (3-MA), 5 μ M wortmannin, 20 nM Baf. A1, 100 nM MG132 for another 24 h. Cell extracts and CM were analyzed by immunoblotting. **g, h** HeLa/WT and FKBPL-CKAP4 DKO cells were left untreated or treated with 1 mM NAV2729 or 100 nM MG132 for 18 h and then treated with 1 μ g/ml DQ-Red-BSA for another 6 h (**g**). Fluorescence signals were observed by fluorescence microscope and analyzed by ImageJ (**h**). Scale bars in (**a**, **d**, and **g**) are 10 μ m. Data represents the mean \pm SEM of three independent experiments in (**c** and **h**). Differences were statistically analyzed by one-way ANOVA followed by Dunnett's multiple comparisons test in (**c** and **h**). Arbitrary units, arb. units.

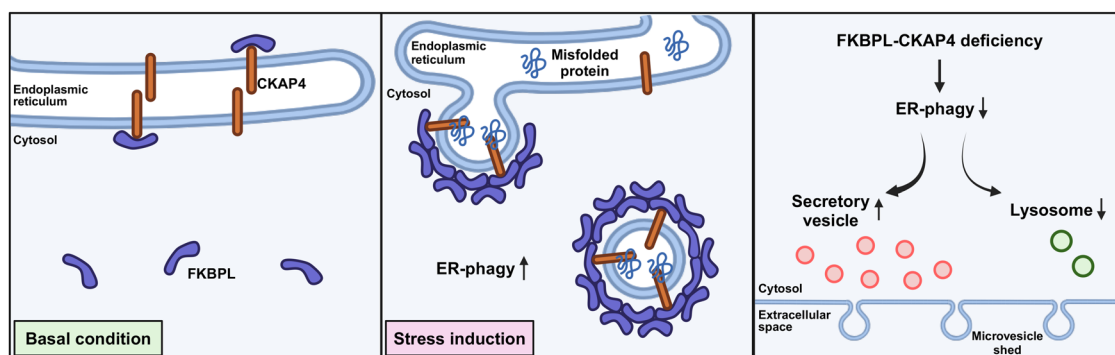


Fig. 8 | Schematic representation of FKBPL-CKAP4-dependent ER-phagy and regulation of protein secretion by its deficiency. Proposed roles of the FKBPL-CKAP4 axis in ER-phagy and protein secretion. In WT cells, ER-phagy-inducing stress induces FKBPL and CKAP4 interaction followed by FKBPL oligomerization, which facilitates ER fragmentation and ER-phagy. FKBPL-CKAP4 deficiency reduces

lysosomal activity and increases in secretory vesicles, leading to non-canonical protein secretion via microvesicle shedding. The illustration created with BioRender.com is released under a Creative Commons Attribution-NonCommercial-NoDerivs 4.0 International license <https://creativecommons.org/licenses/by-nc-nd/4.0/deed.en>.

incubated with primary antibodies (1:200) in PBS-T containing 1% BSA for 4 h, washed with PBS-T four times, and incubated with secondary antibodies (1:500) in PBS-T containing 1% BSA for 1 h. All steps were performed at room temperature. Samples were mounted on cover glass and signals were captured by confocal microscope Leica TSC SP8.

Fractionation

Discontinuous sucrose fractionation with ER enrichment was performed⁵⁴. Briefly, cells were lysed with MTE lysis buffer (270 mM D-mannitol, 10 mM Tris, 0.1 mM EDTA, pH 7.4) containing protease inhibitor cocktail (Quartett) and 1 mM PMSF (Sigma-Aldrich) and sonicated three times, run for 10 sec followed by 10 sec rest intervals. Centrifuged 10 min at 1400 $\times g$, 4 $^{\circ}$ C. Collected 100 μ l supernatant, labeled as “total”. The remaining supernatant was loaded onto discontinuous sucrose layers, composed of 1.3 M, 1.5 M, and 2.0 M sucrose from top to bottom, and ultracentrifuged in 90 Ti (Beckman Coulter) for 70 min at 152,000 $\times g$ 4 $^{\circ}$ C. Upper supernatant were collected and labeled as “cytosol”. “Milky band” at the 1.3 M sucrose was transferred to new tube and ultracentrifuged in 90 Ti (Beckman Coulter) for 45 min at 126,000 $\times g$, 4 $^{\circ}$ C. Resuspended pellet at the bottom and labeled as “ER”. Fractions were added with Laemmli buffer, boiled for 5 min at 95 $^{\circ}$ C, and loaded to SDS-PAGE.

Membrane fractionation with continuous iodixanol gradient was performed⁵⁵. Cells were suspended in a homogenization medium (0.25 M sucrose, 1 mM EDTA, 10 mM HEPES-NaOH, pH 7.4) and homogenized with a 26 G syringe needle 20 times. Centrifuged the homogenate at 1000 $\times g$ for 10 min, 4 $^{\circ}$ C. 0.6 mg of homogenate was layered on top of the continuous 0–30% iodixanol gradient and ultracentrifuged at 200,000 $\times g$ for 2 h, 4 $^{\circ}$ C. Gradients were collected from top to bottom in 12 fractions and added with Laemmli sample buffer, boiled for 5 min at 95 $^{\circ}$ C, and loaded to SDS-PAGE.

Protein topology

Hep3B cells were co-transfected with RFP-KDEL and FKBPL-GFP for 24 h, permeabilized with 0.05% saponin, and digested with 1 μ g/ml trypsin in full medium. Cells were captured by fluorescence microscope Olympus IX71.

Assessment of membrane permeability

Cells were co-stained with membrane permeable reagent acridine orange (OA) (Sigma-Aldrich) and membrane impermeable reagent ethidium bromide (EB) (Sigma-Aldrich) for 10 min. In addition, cells were co-stained with membrane permeable reagent Calcein-AM (Invitrogen) and 1 μ g/ml membrane impermeable reagent propidium iodide (PI) (Sigma-Aldrich) for 10 min. Fluorescence signals were captured by a fluorescence microscope. Cell numbers were counted using CellProfiler.

Transmission electron microscope

Cells were fixed in Karnovsky's fixative buffer, washed three times with 0.05 M sodium cacodylate buffer, and postfixed with 1% osmium tetroxide in 0.1 M sodium cacodylate buffer. Cells were washed three times with distilled water and stained with 0.5% uranyl acetate. After three times washing with distilled water, cells were dehydrated with serially increasing concentration of ethanol and transiently embedded in Spurr's resin. Ultrathin sections were obtained and then observed using a transmission electron microscope JEM1010 (JEOL).

Assessment of lysosomal activity

Cells were incubated with a full medium containing 1 μ g/ml DQ-Red-BSA for 6 h at 37 $^{\circ}$ C and fixed with 4% PFA for 10 min at room temperature. Fluorescence signals were captured by fluorescence microscope Olympus IX71 and analyzed by ImageJ⁵¹.

Assessment of fluorescent intensity and Pearson's correlation coefficient

The fluorescent intensity of each cell was quantified by ImageJ^{53,56}. Each cell was cropped as a region of interest (ROI) and “area, integrated intensity, and mean gray value” were measured using ImageJ. Fluorescent intensity = integrated intensity – selected area * mean gray value of background. Puncta intensity and Pearson's correlation coefficient were analyzed using ImageJ JACoP BIOP⁵⁷. The threshold of each cell was automatically processed with “internodes,” and it appeared in puncta form. Puncta fluorescent intensity was the processed intensity of the puncta. Pearson's correlation coefficient was shown by measuring between channel Green and channel Red.

Statistical analysis

All statistical data were analyzed using GraphPad Prism 9. The intensities of the immunoblotted band and fluorescence intensities were analyzed by ImageJ. Two groups of data were compared with a two-tailed *t* test, and three or more groups of data were compared with one-way ANOVA followed by Dunnett's multiple comparisons test.

Schematic images

Amino acid alignment images were generated with Multalin. Schematic images were generated with BioRender. Protein structures were modified from the Alphafold database.

Reporting summary

Further information on research design is available in the Nature Portfolio Reporting Summary linked to this article.

Data availability

Quantification results and uncropped blots generated in this study are provided in the Source Data file. Fluorescence images generated in this study are provided in the public repository database Figshare (<https://doi.org/10.6084/m9.figshare.25809082>). The raw data of LC-MS/MS analysis are deposited in the ProteomeXchange in the PRIDE database [<http://proteomecentral.proteomexchange.org/cgi/GetDataset?ID=PX034980>]. Source data are provided in this paper.

References

- Jacquemyn, J., Cascalho, A. & Goodchild, R. E. The ins and outs of endoplasmic reticulum-controlled lipid biosynthesis. *EMBO Rep.* **18**, 1905–1921 (2017).
- Schwarz, D. S. & Blower, M. D. The endoplasmic reticulum: structure, function and response to cellular signaling. *Cell. Mol. Life Sci.* **73**, 79–94 (2016).
- Voeltz, G. K., Prinz, W. A., Shibata, Y., Rist, J. M. & Rapoport, T. A. A class of membrane proteins shaping the tubular endoplasmic reticulum. *Cell* **124**, 573–586 (2006).
- Barlowe, C. COPII and selective export from the endoplasmic reticulum. *Biochim. Biophys. Acta Mol. Cell Res.* **1404**, 67–76 (1998).
- Kuehn, M. J., Herrmann, J. M. & Schekman, R. COPII-cargo interactions direct protein sorting into ER-derived transport vesicles. *Nature* **391**, 187–190 (1998).
- Walter, P. & Ron, D. The unfolded protein response: from stress pathway to homeostatic regulation. *Science* **334**, 1081–1086 (2011).
- Chino, H. & Mizushima, N. ER-Phagy: quality control and turnover of endoplasmic reticulum. *Trends Cell Biol.* **30**, 384–398 (2020).
- Hwang, J. & Qi, L. Quality control in the endoplasmic reticulum: crosstalk between ERAD and UPR pathways. *Trends Biochem. Sci.* **43**, 593–605 (2018).
- Meyer, B. A. & Doroudgar, S. ER stress-induced secretion of proteins and their extracellular functions in the heart. *Cells* **9**, 2066 (2020).
- Shaheen, A. Effect of the unfolded protein response on ER protein export: a potential new mechanism to relieve ER stress. *Cell Stress Chaperones* **23**, 797–806 (2018).
- Song, S., Tan, J., Miao, Y. & Zhang, Q. Crosstalk of ER stress-mediated autophagy and ER-phagy: Involvement of UPR and the core autophagy machinery. *J. Cell. Physiol.* **233**, 3867–3874 (2018).
- Johansen, T. & Lamark, T. Selective autophagy: ATG8 family proteins, LIR motifs and cargo receptors. *J. Mol. Biol.* **432**, 80–103 (2020).
- Mizushima, N. A brief history of autophagy from cell biology to physiology and disease. *Nat. Cell Biol.* **20**, 521–527 (2018).
- Khaminets, A. et al. Regulation of endoplasmic reticulum turnover by selective autophagy. *Nature* **522**, 354–358 (2015).
- Fumagalli, F. et al. Translocon component Sec62 acts in endoplasmic reticulum turnover during stress recovery. *Nat. Cell Biol.* **18**, 1173–1184 (2016).
- Grumati, P. et al. Full length RTN3 regulates turnover of tubular endoplasmic reticulum via selective autophagy. *Elife* **6**, e25555 (2017).
- Smith, M. D. et al. CCPG1 is a non-canonical autophagy cargo receptor essential for ER-phagy and pancreatic ER proteostasis. *Dev. Cell* **44**, 217–232. e211 (2018).
- An, H. et al. TEX264 is an endoplasmic reticulum-resident ATG8-interacting protein critical for ER remodeling during nutrient stress. *Mol. Cell* **74**, 891–908. e810 (2019).
- Chen, Q. et al. ATL3 is a tubular ER-phagy receptor for GABARAP-mediated selective autophagy. *Curr. Biol.* **29**, 846–855. e846 (2019).
- Chino, H., Hatta, T., Natsume, T. & Mizushima, N. Intrinsically disordered protein TEX264 mediates ER-phagy. *Mol. Cell* **74**, 909–921. e906 (2019).
- Ji, C. H. et al. The N-degron pathway mediates ER-phagy. *Mol. Cell* **75**, 1058–1072. e1059 (2019).
- Nthiga, T. M. et al. CALCOCO 1 acts with VAMP-associated proteins to mediate ER-phagy. *EMBO J.* **39**, e103649 (2020).
- Zhao, D. et al. A UPR-induced soluble ER-phagy receptor acts with VAPs to confer ER stress resistance. *Mol. Cell* **79**, 963–977 (2020).
- Van Niel, G., d'Angelo, G. & Raposo, G. Shedding light on the cell biology of extracellular vesicles. *Nat. Rev. Mol. Cell Biol.* **19**, 213–228 (2018).
- Zhang, Y., Liu, Y., Liu, H. & Tang, W. (Epub 2019/03/01. <https://doi.org/10.1186/s13578-019-0282-2>.
- Muralidharan-Chari, V. et al. ARF6-regulated shedding of tumor cell-derived plasma membrane microvesicles. *Curr. Biol.* **19**, 1875–1885 (2009).
- Solvik, T. A. et al. Secretory autophagy maintains proteostasis upon lysosome inhibition. *J. Cell Biol.* **221**, e202110151 (2022).
- Kalvari, I. et al. iLIR: A web resource for prediction of Atg8-family interacting proteins. *Autophagy* **10**, 913–925 (2014).
- Xie, Q. et al. hfAIM: A reliable bioinformatics approach for in silico genome-wide identification of autophagy-associated Atg8-interacting motifs in various organisms. *Autophagy* **12**, 876–887 (2016).
- Robson, T. et al. A novel human stress response-related gene with a potential role in induced radioresistance. *Radiat. Res.* **152**, 451–461 (1999).
- Jascur, T. et al. Regulation of p21WAF1/CIP1 stability by WISP39, a Hsp90 binding TPR protein. *Mol. cell* **17**, 237–249 (2005).
- Katayama, H., Kogure, T., Mizushima, N., Yoshimori, T. & Miyawaki, A. A sensitive and quantitative technique for detecting autophagic events based on lysosomal delivery. *Chem. Biol.* **18**, 1042–1052 (2011).
- Sun, N. et al. A fluorescence-based imaging method to measure in vitro and in vivo mitophagy using mt-Keima. *Nat. Protoc.* **12**, 1576–1587 (2017).
- Sanjana, N. E., Shalem, O. & Zhang, F. Improved vectors and genome-wide libraries for CRISPR screening. *Nat. Methods* **11**, 783–784 (2014).
- Birgisdottir, Å. B., Lamark, T. & Johansen, T. The LIR motif—crucial for selective autophagy. *J. Cell Sci.* **126**, 3237–3247 (2013).

36. Lee, S.-Y. et al. APEX fingerprinting reveals the subcellular localization of proteins of interest. *Cell Rep.* **15**, 1837–1847 (2016).
37. Schweizer, A., Rohrer, J., Hauri, H.-P. & Kornfeld, S. Retention of p63 in an ER-Golgi intermediate compartment depends on the presence of all three of its domains and on its ability to form oligomers. *J. Cell Biol.* **126**, 25–39 (1994).
38. Klopfenstein, D. R. et al. Subdomain-specific localization of CLIMP-63 (p63) in the endoplasmic reticulum is mediated by its luminal α -helical segment. *J. Cell Biol.* **153**, 1287–1300 (2001).
39. Nikonov, A. V., Hauri, H.-P., Lauring, B. & Kreibich, G. Climp-63-mediated binding of microtubules to the ER affects the lateral mobility of translocon complexes. *J. Cell Sci.* **120**, 2248–2258 (2007).
40. Li, S.-X., Li, J., Dong, L.-W. & Guo, Z.-Y. Cytoskeleton-Associated Protein 4, a promising biomarker for tumor diagnosis and therapy. *Front. Mol. Biosci.* **7**, 552056 (2021).
41. Jumper, J. et al. Highly accurate protein structure prediction with AlphaFold. *Nature* **596**, 583–589 (2021).
42. Varadi, M. et al. AlphaFold protein structure database in 2024: providing structure coverage for over 214 million protein sequences. *Nucleic Acids Res.* **52**, D368–D375 (2024).
43. Kimura, H. et al. CKAP4 is a Dickkopf1 receptor and is involved in tumor progression. *J. Clin. Invest.* **126**, 2689–2705 (2016).
44. Tagliabracchi, V. S. et al. A single kinase generates the majority of the secreted phosphoproteome. *Cell* **161**, 1619–1632 (2015).
45. Adams, C. J., Kopp, M. C., Larburu, N., Nowak, P. R. & Ali, M. M. Structure and molecular mechanism of ER stress signaling by the unfolded protein response signal activator IRE1. *Front. Mol. Biosci.* **6**, 11 (2019).
46. Yoon, D. et al. Structure-based insight on the mechanism of N-glycosylation inhibition by tunicamycin. *Mol. cells* **46**, 337–344 (2023).
47. Cho, K. F. et al. Proximity labeling in mammalian cells with TurboID and split-TurboID. *Nat. Protoc.* **15**, 3971–3999 (2020).
48. Fujiwara, T., Oda, K., Yokota, S., Takatsuki, A. & Ikehara, Y. Brefeldin A causes disassembly of the Golgi complex and accumulation of secretory proteins in the endoplasmic reticulum. *J. Biol. Chem.* **263**, 18545–18552 (1988).
49. Haupts, U., Maiti, S., Schwille, P. & Webb, W. W. Dynamics of fluorescence fluctuations in green fluorescent protein observed by fluorescence correlation spectroscopy. *Proc. Natl. Acad. Sci. USA* **95**, 13573–13578 (1998).
50. Paroutis, P., Touret, N. & Grinstein, S. The pH of the secretory pathway: measurement, determinants, and regulation. *Physiology* **19**, 207–215 (2004).
51. Zaarur, N. et al. Proteasome failure promotes positioning of lysosomes around the aggresome via local block of microtubule-dependent transport. *Mol. Cell. Biol.* **34**, 1336–1348 (2014).
52. Li, C. et al. Proteasome inhibition activates autophagy-lysosome pathway associated with TFEB dephosphorylation and nuclear translocation. *Front. Cell Dev. Biol.* **7**, 170 (2019).
53. Marwaha, R. & Sharma, M. DQ-Red BSA trafficking assay in cultured cells to assess cargo delivery to lysosomes. *Bio Protoc.* **7**, e2571–e2571 (2017).
54. Williamson, C. D., Wong, D. S., Bozidis, P., Zhang, A. & Colberg-Poley, A. M. Isolation of endoplasmic reticulum, mitochondria, and mitochondria-associated membrane and detergent resistant membrane fractions from transfected cells and from human cytomegalovirus-infected primary fibroblasts. *Curr. Protoc. Cell Biol.* **68**, 3.27. 21–23.27. 33 (2015).
55. Graham, J. Fractionation of Golgi, endoplasmic reticulum, and plasma membrane from cultured cells in a preformed continuous iodoxanol gradient. *Sci. World J.* **2**, 1435–1439 (2002).
56. Schindelin, J. et al. Fiji: an open-source platform for biological-image analysis. *Nat. Methods* **9**, 676–682 (2012).
57. Bolte, S. & Cordelières, F. P. A guided tour into subcellular colocalization analysis in light microscopy. *J. Microsc.* **224**, 213–232 (2006).

Acknowledgements

We would like to thank Dr. Noboru Mizushima (Tokyo University, Japan) for ssRFP-EGFP-KDEL construct and HeLa/ssRFP-EGFP-KDEL WT, FIP200 KO and TEX264 KO cells, Dr. Jin-A Lee (Hannam University, Korea) and Yong-Woo Jun (Kyungpook National University, Korea) for mRFP-tagged LC3/GABARAP constructs, Dr. Atsushi Miyawaki (RIKEN, Japan) for mt-mKeima construct, Dr. Feng Zhang (MIT) for CRISPR-Cas9 constructs, and Dr. Hyun-Woo Rhee (Seoul National University, Korea) for biotin ligase vector V5-APEX2. This work was supported by the Korea Health Technology R&D Project (RS-2020-KH107190, RS-2023-KH134817) through the Korea Health Industry Development Institute (KHIDI) and Korea Dementia Research Center (KDRC), funded by the Ministry of Health & Welfare and Ministry of Science and ICT, and a CRI grant (NRF-2022R1A2B5B03001249) funded by the Ministry of Education, Science and Technology, Korea.

Author contributions

C.M.L. and Y.-K.J. designed the study. C. M. L. performed most experiments; C.M.L. and J. K. performed immunocytochemistry assay; C. M. L., J. K., and J. B. performed quantitation analysis; C. M. L. and Y. K. performed immunoprecipitation assay, C. M. L. and H. P. generated plasmid constructs; C. M. L. and Y.-K.J. analyzed data and wrote the manuscript.

Competing interests

The authors declare no competing interests.

Additional information

Supplementary information The online version contains supplementary material available at <https://doi.org/10.1038/s41467-024-52188-7>.

Correspondence and requests for materials should be addressed to Yong-Keun Jung.

Peer review information *Nature Communications* thanks the anonymous reviewer(s) for their contribution to the peer review of this work. A peer review file is available.

Reprints and permissions information is available at <http://www.nature.com/reprints>

Publisher's note Springer Nature remains neutral with regard to jurisdictional claims in published maps and institutional affiliations.

Open Access This article is licensed under a Creative Commons Attribution-NonCommercial-NoDerivatives 4.0 International License, which permits any non-commercial use, sharing, distribution and reproduction in any medium or format, as long as you give appropriate credit to the original author(s) and the source, provide a link to the Creative Commons licence, and indicate if you modified the licensed material. You do not have permission under this licence to share adapted material derived from this article or parts of it. The images or other third party material in this article are included in the article's Creative Commons licence, unless indicated otherwise in a credit line to the material. If material is not included in the article's Creative Commons licence and your intended use is not permitted by statutory regulation or exceeds the permitted use, you will need to obtain permission directly from the copyright holder. To view a copy of this licence, visit <http://creativecommons.org/licenses/by-nc-nd/4.0/>.

© The Author(s) 2024